Incoherent Tunneling on Ni(111) Surface

Matthew Ord

Abstract

A first principles approach was used to model the incoherent ground state to ground state tunneling of hydrogen on a Ni(111) surface.

Through the application of the Lindblad equation the model was used to produce an equation describing the evolution of the hydrogen density matrix

$$\langle m|\,\dot{\hat{\rho}}(t)\,|m\rangle = 2\sum_{n\neq m}[\Gamma_{m,n;m,n}(\omega_{m,n})\rho_{n,n} - \Gamma_{n,m;n,m}(\omega_{n,m})\rho_{m,m}] \quad (1)$$

where

$$\Gamma_{i,j,k,l}(\omega_{k,l}) = \exp{(\frac{\beta\omega_{k,l}}{2})}\mathcal{C}_{i,j}\mathcal{C}_{k,l}\sqrt{\pi}\frac{32k_f^2\epsilon_0^2\hbar^3}{\beta e^4 m_e^2} \quad (2)$$

$\omega_{i,j} = E_i - E_j$, E_i is the energy of the hydrogen at site i and k_f is the fermi wavevector of nickel. Previous DFT calculations were used to find the hydrogen overlap fraction $\mathcal{C}_{i,j}$ where i, j denotes either a low energy FCC or a high energy HCP site. Analysis of the combined FCC and HCP occupation gave an expression for the tunneling rate R

$$R = 12\cosh{(\frac{\beta\omega_{k,l}}{2})}\mathcal{C}_{1,0}\mathcal{C}_{0,1}\sqrt{\pi}\frac{32k_f^2\epsilon_0^2\hbar^3}{\beta e^4 m_e^2} \quad (3)$$

where the FCC-HCP overlap of nickel $\mathcal{C}_{1,0}$ was found to be $\sim 4.4\times10^{-3}$. Calculations at $150K$ gave a rate of $1.8\times10^9 s^{-1}$. The rate was also measured from the initial site occupation ($2.5\times10^9 s^{-1}$), HCP occupation ($2.3\times10^9 s^{-1}$) next FCC occupation ($1.5\times10^9 s^{-1}$) and mean-squared distance ($2.0\times10^9 s^{-1}$) which were also shown to be constant with experiment.

The full electron-hydrogen dynamics were investigated through direct integration of the Schrödinger equation. Data extracted from the simulation predicted a tunneling rate of $4.3\pm0.1\times10^9 s^{-1}$ at 150K, which was again consistent with experiment. Comparison between the behaviour of the simulation and Lindblad analysis found many similarities between the predicted hydrogen dynamics.

1 Introduction

The aim of this report is to investigate the extent to which a first-principles calculation could be used to predict the rate of incoherent ground state to ground state tunneling of hydrogen on the surface of nickel.

Hydrogen diffusion has been measured on the surface of Ni(111) through many different techniques[16, 4], most recently using Helium-3 spin-echo interferometry[12]. With the help of first-principle DFT calculations of the H-Ni(111) potential a quantum version of transition state theory (ASTST) was developed to describe these tunneling rates[24]. The results of this theory were found to closely match the predicted hopping rates, particularly when the rate was dominated by activated tunnelling[24]. There was however a difference in the rate at low temperatures, where it is thought that interaction with the electron gas leads to incoherent tunnelling. This type of interaction is of particular relevance in the development of superconducting interference devices (SQUIDs)[21] and has been successfully described through the introduction of effective dissipative models[3]. To be able to assess this approach however it is first necessary to investigate the propagation of hydrogen directly by introducing a model of the complete electron-hydrogen interaction.

To find an effective theory describing only the system we can trace out the environmental degrees of freedom to produce a quantum master equation. Initial attempts to find such an equation by Redfield[20] and Lamb[14] produce many useful results, however in general they do not preserve the trace of the density matrix[6]. This issue was eventually solved through the introduction of the Lindblad equation, developed by Lindblad[17] and simultaneously by V. Gorini et al. [10].

A model for the electron-hydrogen interaction is outlined in section 2, which is used alongside the Lindblad equation to find an analytical prediction of the tunnelling rate in section 3. In sections 4 and 5 the behaviour of the system was also investigated through direct integration of the Schrödinger equation, including both the dynamics of the system and the environment. The similarities and limitations of the two methods are discussed in section 6 before the conclusions of the report are outlined in section 7.

2 The Model

We will focus on a model of electron-hydrogen interaction within a nickel lattice arranged in a face centred cubic structure. The hydrogen atom occupies hollow sites within nickel[10], which are arranged in a honeycomb configuration (fig. 1a). Due to interaction with atoms below the surface we find these sites are split into alternating low energy FCC and high energy HCP sites[24]. To calculate

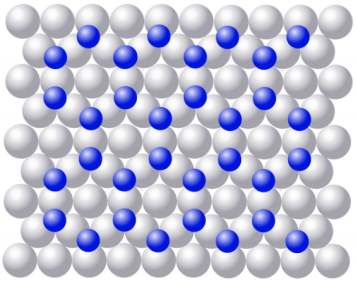

(a) Arrangement of Hydrogen Sites

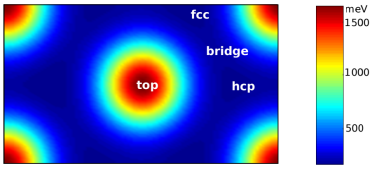

(b) DFT Potential surface

Figure 1: Arrangement of hydrogen sites on a Ni(111) surface,alternating between low energy FCC and high energy HCP sites arranged in a honeycomb structure. figs. 1a and 1b are reproductions of those found in[24]

the incoherent rate of tunneling between the FCC and HCP ground states we need to find a hamiltonian to describe the combined electron-hydrogen system. The electron-hydrogen system can be described by a combination of a free and interaction hamiltonian

$$\hat{H} = \hat{H}_{free} + \hat{H}_{int} \tag{4}$$

where the free hamiltonian $\hat{H}_{free}$ can be separated into an electron and hydrogen component

$$\hat{H}_{free} = \hat{H}_{e^-} + \hat{H}_h \tag{5}$$

2.1 Electron States

Ignoring the interaction between the electrons and the lattice as well as electron-electron interactions we can expand the free electron hamiltonian in the plane wave basis

$$\hat{H}_{e^-} = \sum_{k,s} \frac{\hbar^2 k^2}{2m_e} \hat{b}^\dagger_{k,s} \hat{b}_{k,s} \tag{6}$$

where $\hat{b}^\dagger_{k,s}$ is the electron creation operator with spin s and wavevector k satisfying the standard fermion anti-commutation relations $\{\hat{b}_{k,s}, \hat{b}^\dagger_{k',s'}\} = \delta_{kk'}\delta_{ss'}$.

Taking the lattice constant of nickel as $3.499 \pm 0.005 \times 10^{-10} m$ [8], we find a density of $9.34 \pm 0.04 \times 10^{28} m^{-3}$. If both of the 2 valence electrons on nickel

are completely delocalised we find an electron density of $n = 1.87 \times 10^{29} m^{-3}$. This is used to calculate the fermi-wavevector and fermi-energy of nickel [13]

$$\epsilon_f = \frac{\hbar^2}{2m}(3\pi^2 n)^{2/3} \tag{7}$$

$$= 1.91 \times 10^{-18} J \tag{8}$$

$$k_f = (3\pi^2 n)^{\frac{1}{3}} \tag{9}$$

$$= 1.77 \times 10^{10} m^{-1} \tag{10}$$

From measurements of the optical properties of nickel the fermi energy is found to be slightly lower at only $1.24 \times 10^{-18} J$ [9].

2.2 Hydrogen States

For hydrogen we make use of the eigenstates found in the previous DFT analysis[24].

$$\hat{H}_h = E_0 \sum_{i \exists fcc} \hat{a}_i^\dagger \hat{a}_i + E_1 \sum_{i \exists hcp} \hat{a}_i^\dagger \hat{a}_i \tag{11}$$

where E_0 is the energy of an FCC site and E_1 is the energy of a HCP site. $\hat{a}_i^\dagger$ is the hydrogen creation operator for the site i which satisfies the standard commutation relations for a boson $\left[\hat{a}_i, \hat{a}_j^\dagger\right] = \delta_{ij}$.

Although DFT calculations also provide a theoretical prediction of the hydrogen energies, the energy used in the model were taken from direct spin-echo measurements of the surface[24]

$$\Delta E_{hyd} = E_1 - E_0 = 3.04 \pm 0.16 \times 10^{-21} J \tag{12}$$

2.3 Electron Hydrogen Interaction

To describe the electron-hydrogen interaction we introduce field operators $\hat{\psi}_e$ and $\hat{\psi}_h$ [19]

$$\hat{H}_{int} = \int\int d\mathbf{r} d\mathbf{r}' V(\mathbf{r} - \mathbf{r}') \hat{\psi}_h^\dagger(\mathbf{r}) \hat{\psi}_e^\dagger(\mathbf{r}') \hat{\psi}_e(\mathbf{r}') \hat{\psi}_h(\mathbf{r}) \tag{13}$$

where $V(\mathbf{r})$ is the electron-hydrogen interaction potential. We expand out the electron operator in the free electron basis state

$$\hat{\psi}_e(\mathbf{r}) = \sum_{k,s} \langle \mathbf{r} | \mathbf{k} \rangle \hat{b}_{k,s} \tag{14}$$

$$= \frac{1}{L^{\frac{3}{2}}} \sum_{k,s} \exp\left(i\mathbf{k}.\mathbf{r}\right) \hat{b}_{k,s} \tag{15}$$

to give us the expression

$$\hat{H}_{int} = \sum_{k,s,k',s'} \int\int \frac{d\mathbf{r}d\mathbf{r}'}{L^3} V(\mathbf{r}-\mathbf{r}')\hat{b}^\dagger_{k',s'}\hat{b}_{k,s} \exp\left(i(\mathbf{k}-\mathbf{k}').\mathbf{r}'\right)\hat{\psi}^\dagger_h(\mathbf{r})\hat{\psi}_h(\mathbf{r}) \quad (16)$$

$$= \frac{1}{L^3}\sum_{k,s,k',s'} \int d(\mathbf{r}'-\mathbf{r})V(\mathbf{r}-\mathbf{r}')\hat{b}^\dagger_{k',s'}\hat{b}_{k,s} \exp\left(i(\mathbf{k}-\mathbf{k}').(\mathbf{r}'-\mathbf{r})\right) \quad (17)$$

$$\int d\mathbf{r} \exp\left(i(\mathbf{k}-\mathbf{k}').\mathbf{r}\right)\hat{\psi}^\dagger_h(\mathbf{r})\hat{\psi}_h(\mathbf{r})$$

$$\hat{H}_{int} = \frac{1}{L^3}\sum_{k,s,k',s'} \hat{b}^\dagger_{k',s'}\hat{b}_{k,s}\tilde{V}(\mathbf{q}) \int d\mathbf{r}\hat{\psi}^\dagger_h\hat{\psi}_h \exp(i\mathbf{q}.\mathbf{r}) \quad (18)$$

If we also expand the hydrogen creation operator

$$\hat{\psi}_h(\mathbf{r}) = \sum_i \psi_{h,i}(\mathbf{r})\hat{a}_i \quad (19)$$

we find

$$\hat{H}_{int} = \frac{1}{L^3}\sum_{\substack{k,s,k',s'\\i,j}} \hat{b}^\dagger_{k',s'}\hat{b}_{k,s}\hat{a}^\dagger_i\hat{a}_k\tilde{V}(\mathbf{q}) \int d\mathbf{r}\psi^*_{h,i}(\mathbf{r})\psi_{h,j}(\mathbf{r}) \exp(i\mathbf{q}.\mathbf{r}) \quad (20)$$

where $\mathbf{q} = \mathbf{k}-\mathbf{k}'$ is the scattering wavevector, and $\tilde{V}(\mathbf{q})$ is the fourier transform of the interaction potential.

2.4 The Electron Hydrogen Potential

The interaction potential can be found from the greens function of the coulomb equation [1]

$$V(\mathbf{r}) = \frac{e^2}{4\pi\epsilon_0}(-\frac{1}{r} + \int \frac{|\psi(\mathbf{r}')|^2}{|\mathbf{r}-\mathbf{r}'|}d\mathbf{r}') \quad (21)$$

Electrons surrounding the hydrogen atom have energies $E_n = -\frac{13.6}{n^2}eV$ [11]. Since the energy required to excite the electron to the $n = 2$ energy level is much greater than the fermi energy of Ni ($7.76eV$) [9] we can make the approximation that the electron surrounding the hydrogen lie close to the 1s ground state. This corresponds to a wavefunction[11]

$$\psi(\mathbf{r}) = (\pi a_0^3)^{-1/2} e^{-\frac{r}{a_0}} \quad (22)$$

where a_0 is the bohr radius. We then fourier transform this expression (see appendix A) to find

$$\tilde{V}(\mathbf{q}) = \frac{e^2}{\epsilon_0 q^2}(\frac{\alpha^4}{(\alpha^2+q^2)^2} - 1) \quad (23)$$

with $\alpha = \frac{2}{a_0}$. If we expand about $q = 0$ we find

$$\tilde{V}(q) \sim \frac{e^2}{\epsilon_0 q^2}(1 - 2(\frac{q}{\alpha})^2 + 3(\frac{q}{\alpha})^4 - 1) \tag{24}$$

$$= -\frac{2e^2}{\epsilon_0 \alpha^2}(1 - \frac{3}{2}(\frac{q}{\alpha})^2) + \mathcal{O}(q^4) \tag{25}$$

taking $q = k_f = 1.77 \times 10^{10} m^{-1}$ (see section 2.1) and $\alpha = 3.79 \times 10^{10}$ we see the second order correction only contributes to a variation of around 14.5%. We therefore assume that for the relevant scattering of electrons the potential takes a constant value $\tilde{V}(q) \sim -\frac{2e^2}{\epsilon_0 \alpha^2}$.

2.5 The Hydrogen Wavefunction

The final term in eq. (20) involves the integral of the product of the two hydrogen wavefunctions. Previous DFT calculations gave the form of bloch wavefunctions spread throughout the whole material[24], so to recover a localised wavepacket several of these states were chosen centered about $q = 0$. Given the localised wavefunction it was possible to calculate the fourier transform products directly. The fourier transform was seen to oscillate (fig. 2) at a frequency proportional to $\frac{2\pi}{a}$ where a is the lattice constant of Ni. The value of this constant is around $3.499 \pm 0.005 \times 10^{-10} m$ [8] corresponding to oscillations at $q = 1.79 \pm 0.03 \times 10^{10} m^{-1}$ which in theory should have a noticeable effect on the matrix element, with a fermi wavevector of $1.177 \times 10^{10} m^{-1}$ eq. (10). In a real material we

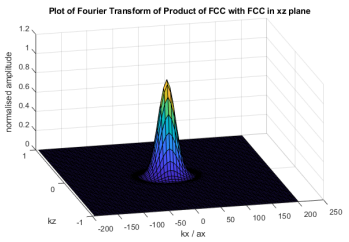

(a) FCC-FCC Fourier Transform in xz Plane

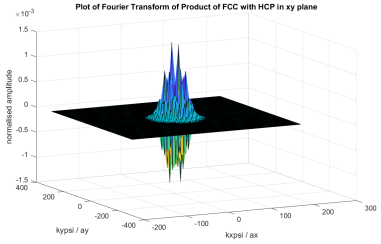

(b) FCC-HCP Fourier Transform in xy Plane

Figure 2: Results of the hydrogen fourier transform calculations. FCC-FCC and HCP-HCP calculations (fig. 2a) show a smooth curve, with a normalised value of 1 at $q = 0$. The FCC-HCP fourier transform (fig. 2b) however show oscillations with a characteristic wavevector $q = 1.79 \pm 0.03 \times 10^{10} m^{-1}$, corresponding to the lattice vector of Ni.

should expect the nickel atoms to oscillate which would break the fixed distance between FCC and HCP sites. The individual peaks are therefore simply a side effect of the DFT analysis.

Since the overall wavepacket decays over a region of around $\frac{100\pi}{a}$ we should be able to ignore the oscillations of $V(\mathbf{q})$ to obtain an effective constant potential

required for the simulation. For this model we simply take the maximum overlap of the normalised wavefunction (table 1).

Overlap	Maximum Overlap	Normalised Overlap
FCC-FCC	3.00×10^7	1
HCP-HCP	3.00×10^7	1
HCP-FCC	1.33×10^5	4.4×10^{-3}

Table 1: Normalised Hydrogen overlaps as used in the model. Fluctuations in the overlap integral are ignored. The maximum is taken instead of the $q = 0$ value as the HCP-FCC integral has a minimum at this point.

2.6 Simplified Electron-Hydrogen Interaction

For simplicity we introduce an effective potential $\tilde{V}(\mathbf{q})_{i,j}$ where

$$\hat{H}_{int} = \sum_{k,s,k',s',i,j} \tilde{V}(\mathbf{q})_{i,j} \hat{b}^\dagger_{k',s'} \hat{b}_{k,s} \hat{a}^\dagger_i \hat{a}_j \tag{26}$$

If we take the potential to be independent of q we can separate it into a constant prefactor and hydrogen overlap factors

$$V_{i,j} = \frac{1}{L^3} \mathcal{C}_{i,j} \frac{2e^2}{\epsilon_0 \alpha^2} \tag{27}$$

$$= \frac{1}{L^3} \mathcal{C}_{i,j} \frac{8\pi^2 \epsilon_0 \hbar^4}{e^2 m_e^2} \tag{28}$$

where $\mathcal{C}$ takes the value

$$\mathcal{C}_{i,i} = 1 \tag{29}$$

$$\mathcal{C}_{i,\neq i} = 0.0044 \tag{30}$$

It is often beneficial to separate eq. (26) into a system and environment contribution.

$$\hat{H}_{int} = \sum_{i,j} \hat{a}^\dagger_i \hat{a}_j \sum_{k,s,k',s'} \tilde{V}_{i,j} \hat{b}^\dagger_{k',s'} \hat{b}_{k,s} \tag{31}$$

$$= \sum_{i,j} \hat{S}_{i,j} \hat{E}_{i,j} \tag{32}$$

where

$$\hat{S}_{i,j} = \hat{a}^\dagger_i \hat{a}_j \tag{33}$$

$$\hat{E}_{i,j} = \sum_{k,s,k',s'} \tilde{V}_{i,j} \hat{b}^\dagger_{k',s'} \hat{b}_{k,s} \tag{34}$$

3 Lindblad Equation

3.1 General Equation of Motion

The state of the electron hydrogen system can be completely characterised by its density matrix. Working in the interaction picture, a general density matrix $\hat{\rho}(t)$ time evolves according to the von Neumann equation[15]

$$\frac{d\hat{\rho}_t(t)}{dt} = -i[\hat{H}_{int}(t), \hat{\rho}_t(t)] \tag{35}$$

which can be integrated to give

$$\hat{\rho}_t(t) = \hat{\rho}_t(0) - i\int_0^t ds[\hat{H}_{int}(s), \hat{\rho}_t(s)] \tag{36}$$

We can expand this equation of motion to second order in the interaction by substituting eq. (36) into eq. (35) twice to give

$$\frac{d\hat{\rho}_t(t)}{dt} = -i[\hat{H}_{int}(t), \hat{\rho}_t(0)] - \int_0^t ds[\hat{H}_{int}(t), [\hat{H}_{int}(s), \hat{\rho}_t(t)]] + \mathcal{O}(\hat{H}^3_{int}) \tag{37}$$

We reduce this to an equation describing the density operator of the system $\hat{\rho}(t) = Tr_e[\hat{\rho}_t(t)]$ by taking a trace over the environment[18]

$$\hat{\rho}(t) = -iTr_e[\hat{H}_{int}(t), \hat{\rho}_t(0)] - \int_0^t dsTr_e[\hat{H}_{int}(t), [\hat{H}_{int}(s), \hat{\rho}_t(t)]] \tag{38}$$

Using a clever re-definition of the interaction Hamiltonian [18] it is possible to show that the first term gives no contribution to the overall dynamics.

3.2 The Redfield Equation

We make the assumption that the system and surrounding density matrix is completely decoupled [2]

$$\hat{\rho}_t(t) = \hat{\rho}(t) \otimes \hat{\rho}_E(0) \tag{39}$$

where $\hat{\rho}_E(t)$ is the density matrix of the environment. Under the Markov approximation we then extend the upper limit of eq. (38) to ∞, arriving at the Redfield equation

$$\dot{\hat{\rho}}(t) = -\int_0^\infty dsTr_E[\hat{H}_{int}(t), [\hat{H}_{int}(s-t), \hat{\rho}(t) \otimes \hat{\rho}_E(0)]] \tag{40}$$

Separating out the interaction hamiltonian into system and surroundings according to eq. (32)

$$\hat{H}_{int} = \sum_{i,j} \hat{S}_{i,j}\hat{E}_{i,j} \tag{41}$$

we can simplify the form of this equation[18] to give

$$\dot{\hat{\rho}}(t) = \sum_{i,j,k,l} \exp\left(-i(\omega_{i,j} - \omega_{k,l})t\right)\Gamma_{i,j;k,l}(\omega_{k,l})[S_{k,l}\hat{\rho}(t), S^{\dagger}_{i,j}] \\ + \exp\left(i(\omega_{i,j} - \omega_{k,l})\right)\Gamma^{*}_{k,l;i,j}(\omega_{i,j})[S_{k,l}, \hat{\rho}(t)S^{\dagger}_{i,j}] \tag{42}$$

where Γ is the Lindblad rate constant given by

$$\Gamma_{i,j,k,l}(\omega) = \int_0^{\infty} ds \exp\left(i\omega s\right) Tr_E[E^{\dagger}_{i,j}(t)E_{k,l}(t-s)\rho_E(0)] \tag{43}$$

3.3 The Lindblad Equation

To proceed we first expand out the commutators

$$\langle m| \left[S_{k,l}\hat{\rho}(t), S^{\dagger}_{i,j}\right] |n\rangle = \sum_{\alpha,\beta} \rho_{\alpha,\beta}[\delta_{m,k}\delta_{l,\alpha}\delta_{\beta,j}\delta_{i,n} - \delta_{m,j}\delta_{i,k}\delta_{l,\alpha}\delta_{\beta,n}] \tag{44}$$

$$\langle m| \left[S_{k,l}, \hat{\rho}(t)S^{\dagger}_{i,j}\right] |n\rangle = \sum_{\alpha,\beta} \rho_{\alpha,\beta}[\delta_{m,k}\delta_{l,\alpha}\delta_{\beta,j}\delta_{i,n} - \delta_{m,\alpha}\delta_{\beta,j}\delta_{i,k}\delta_{l,n}] \tag{45}$$

which we use to obtain an expanded form

$$\langle m| \dot{\hat{\rho}}(t) |n\rangle = \sum_{i,j,k,l,\alpha,\beta} \exp\left(-i\Delta E t\right)\Gamma_{i,j;k,l}(\omega_{k,l})\rho_{\alpha,\beta}[\dots] \\ + \exp\left(i\Delta E t\right)\Gamma^{*}_{k,l;i,j}(\omega_{i,j})\rho_{\alpha,\beta}[\dots] \tag{46}$$

where $\Delta E = \omega_{i,j} - \omega_{k,l}$. To arrive at the Lindblad equation (eq. (128)) we apply the rotating wave approximation which is imposed using the expression $\delta_{i,j}\delta_{k,l} + \delta_{i,k}\delta_{j,l} - \delta_{i,j}\delta_{k,l}\delta_{i,k}$

$$\langle m| \dot{\hat{\rho}}(t) |m\rangle = 2\sum_{n \neq m} [\Gamma_{m,n;m,n}(\omega_{m,n})\rho_{n,n} - \Gamma_{n,m;n,m}(\omega_{n,m})\rho_{m,m}] \tag{47}$$

where we sum over all neighbouring sites $n \neq m$. Note that the off diagonal terms vanish assuming the density matrix is initially purely diagonal. A full derivation can be found in appendix C.

3.4 Lindblad Rate Constant

Using eq. (43) we can calculate the value of the Lindblad rate constant (Γ). If we assume the electrons are initially in a purely statistical ensemble the density matrix is given by[22]

$$\rho_E(0) = \sum_{\{N(k)\}} P(\{N(k)\}) \left|N(k)\right\rangle \left\langle N(k)\right| \tag{48}$$

using the definition of $\hat{E}_{i,j}$ given in section 2.6 we can take the trace over the environment (see appendix D)

$$Tr_E[\dots] = \sum_{\substack{\{N(k)\} \\ k_1,s^1,k_2,s^2 \\ k_3,s^3,k_4,s^4}} P(\{N(k)\})V_{i,j}V_{k,l} \exp\left(i(E_1-E_2)t\right)\exp\left(i(E_3-E_4)(t-s)\right) \langle N(k)|\, \hat{b}^\dagger_{k_1,s^1}\hat{b}_{k_2,s^2}\hat{b}^\dagger_{k_3,s^3}\hat{b}_{k_4,s^4}\,|N(k)\rangle \tag{49}$$

where $\{N(k)\}$ is the set of all possible occupations, and the boltzmann probability associated with a given state is $P(\{N(k)\}) = \exp\left(-\beta(E-\mu N)\right)$. The trace is only non zero in two cases

- $k_1 = k_2, s^1 = s^2$, $k_3 = k_4, s^3 = s^4$
- $k_1 = k_4, s^1 = s^4$, $k_3 = k_2, s^3 = s^2$ but $k_1 \neq k_2, s^1 \neq s^2$

which we use to simplify eq. (49)

$$Tr_E[\dots] = \sum_{k_1,s^1,k_3,s^3} V_{i,j}V_{k,l}[N_1N_3 + N_1(1-N_3)\exp\left(-i(E_3-E_1)s\right)] \tag{50}$$

Integrating over s we obtain an additional constraint on k_3 in the form of energy conservation. After converting the sum into an integral we re-adsorb the power of L^3 into the definition of $V_{i,j}$ (see section 2.6) to give

$$\Gamma_{i,j,k,l}(\omega) = \sum_{s^1,s^3}\int \frac{d^3\mathbf{k}_1}{(2\pi)^3}\frac{d^3\mathbf{k}_3}{(2\pi)^3}V_{i,j}V_{k,l}[N_1N_3\delta_{w,0}\frac{m_e}{\sqrt{k_3^2}} + N_1(1-N_3)\frac{m_e}{\sqrt{k_1^2-2m_e\omega}}\delta(k_3 \pm \sqrt{k_1^2+2m_e\omega})] \tag{51}$$

The first term is divergent, however since we find no terms in the Redfield equation with $\omega = 0$ it does not contribute to tunneling (appendix D.1). We evaluate the second term by expanding the integrand about the fermi wavevector

$$\frac{k_1^2k_3^2N_1(1-N_3)}{\sqrt{k_1^2-2m_e\omega}}\delta(\dots) \sim \frac{k_1^3N_1(1-N_1)}{4}\exp\left(\frac{\beta\omega}{2}\right)\exp\left(-\frac{(\beta\Delta E)^2}{4}\right) \tag{52}$$

where $\Delta E = E_1 - E_f$. Although the form of the expansion does not exactly match up with the actual integrand (fig. 3) the approximate integral comes to within 3% of the true value. Applying this approximation we find

$$\Gamma_{i,j,k,l}(\omega_{k,l}) = \sum_{s^1,s^3}\exp\left(\frac{\beta\omega_{k,l}}{2}\right)\frac{m_ek_f^2}{(2\pi)^4}V_{i,j}V_{k,l}\sqrt{\pi}\frac{2m_e}{\beta\hbar^2} \tag{53}$$

Substituting in the expression for $V_{i,j}$ we arrive at the final expression for Γ

$$\Gamma_{i,j,k,l}(\omega_{k,l}) = \exp\left(\frac{\beta\omega_{k,l}}{2}\right)\mathcal{C}_{i,j}\mathcal{C}_{k,l}\sqrt{\pi}\frac{32k_f^2\epsilon_0^2\hbar^3}{\beta e^4{m_e}^2} \tag{54}$$

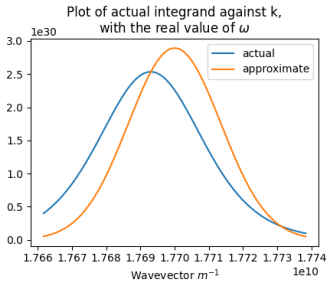

(a) Approximation for Experimental ω

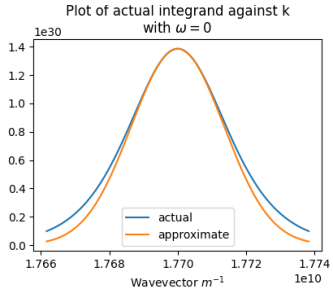

(b) Approximation for $\omega = 0$

Figure 3: Plot of the integrand for $\omega = 0$ (fig. 3a) and the experimental ω (fig. 3b). Although the expanded form is shifted for the real value of ω the integral agrees to within 3%.

3.5 Two Sites

Since eq. (47) is a simple rate equation it is possible to solve it analytically for a system with one HCP and one FCC site (appendix B). We find the forward and backward tunnelling rate

$$\gamma_0 = 2\Gamma_{1,0;0,1}(\omega_{1,0}) \tag{55}$$

$$= A \exp\left(\frac{\beta\omega_{0,1}}{2}\right)\mathcal{C}_{1,0}\mathcal{C}_{0,1} \tag{56}$$

$$\gamma_1 = 2\Gamma_{0,1;1,0}(\omega_{0,1}) \tag{57}$$

$$= A \exp\left(\frac{\beta\omega_{1,0}}{2}\right) \tag{58}$$

$$\tag{59}$$

where $A = \mathcal{C}_{1,0}\mathcal{C}_{0,1}\sqrt{\pi}\frac{64k_f^2\epsilon_0^2\hbar^3}{\beta e^4 m_e^2}$. This gives a combined rate of

$$R = \gamma_0 + \gamma_1 = 2A\cosh\left(\frac{\beta(E_1 - E_0)}{2}\right) \tag{60}$$

for an energy difference of $3.04 \pm 0.16 \times 10^{-21}J$ (eq. (12)) we find a tunnelling rate of $6.1 \times 10^8 s^{-1}$, corresponding to a tunnelling time of $1.6 \times 10^{-9}s$ at $150K$.

3.6 Multiple Sites

In reality as there are 3 HCP sites neighbouring each FCC Hydrogen the rate at which the combined occupation reaches the boltzmann distribution is exactly 3 times the single neighbour rate (see section 2).

$$R = 6A\cosh\left(\frac{\beta(E_1 - E_0)}{2}\right) \tag{61}$$

where $R = 1.8 \times 10^9 s^{-1}$ at $150K$. It is also possible to infer a tunneling rate

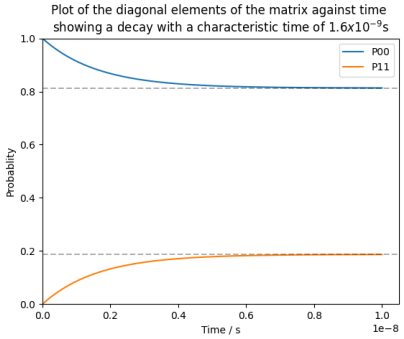

Figure 4: Plot of the Lindblad solution with a characteristic decay rate of $6.1 \times 10^8 s^{-1}$ at $150K$.

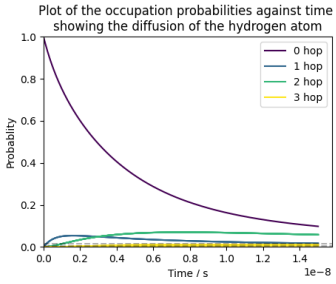

(a) Individual occupation probability

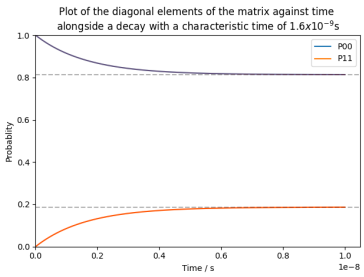

(b) Combined occupation probability

Figure 5: Plot of the individual and combined occupation probabilities against time at $150K$. The combined probability (fig. 5b) follows exactly the same curve as in fig. 4 with a rate of $1.8 \times 10^9 s^{-1}$. The plot of the individual occupation probabilities (fig. 5a) shows that it takes a much longer time for the probability of occupation of the initial site to reach an equilibrium with the surroundings.

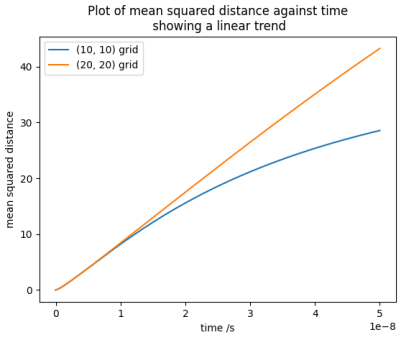

Figure 6: Plot of the squared distance of the hydrogen atom against time showing a linear trend as expected for a random walk. The time taken for the rms distance to equal 0.5 is found to be $5.09 \times 10^{-10} s$, which corresponds to an implied rate of $2.0 \times 10^{9} s^{-1}$.

from the time taken for individual probability distributions to reach equilibrium (fig. 5a). For the initial FCC site we can take this equilibrium value to be either zero, or the boltzmann equilibrium. We can also use the time taken for the neighbouring HCP sites to reach their maximum occupation. The corresponding decay times are given in table 2.

Measure	Decay Time s	Implied Decay Rate s^{-1}
Initial FCC	4.54×10^{-9}	2.2×10^{8}
Initial FCC (Boltzmann)	3.99×10^{-10}	2.5×10^{9}
Next HCP	4.37×10^{-10}	2.3×10^{9}
Next FCC	$4 \times 6.55 \times 10^{-10}$	1.5×10^{9}
Combined Occupation	5.56×10^{-10}	1.8×10^{9}
RMS Distance	5.09×10^{-10}	2.0×10^{9}

Table 2: Implied decay rates from the probability distribution and RMS distance at $150K$. The RMS decay time corresponds to the time for the RMS distance to equal 0.5. The implied decay time taken for the next FCC site is taken to be $\frac{1}{4}$ the time to equilibrium, as the time taken grows as distance squared. Most measures of the decay rate take a similar amount of time, however the complete decay of the FCC occupation takes an order of magnitude longer.

3.7 Distance Traveled

We should also be able to extract a tunneling time from the root-mean squared (rms) distance travelled by the hydrogen. As the hydrogen undergoes a random walk we should expect the squared distance to grow linearly with time. The

tunneling time was found to be $5.25 \times 10^{-10} s$, corresponding to the time taken for the rms distance to reach 0.5 As time grows as distance squared a tunneling rate was also extracted from $\frac{1}{4}$ the neighbouring FCC equilibrium time.

3.8 Comparison with Experiment

Given these measures of the tunneling time it is now possible to compare these tunneling rates to experiment. In fig. 7 the theoretical rates are plotted against temperature alongside the rates extracted from the Lindblad analysis. The FCC

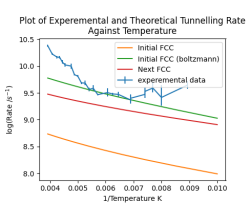

(a) FCC Tunneling Rates

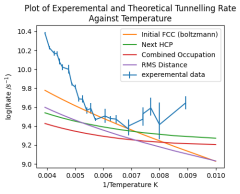

(b) Non-FCC Tunneling Rates

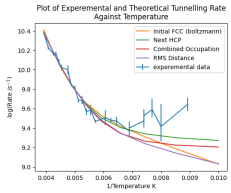

(c) Combined Tunneling Rate

Figure 7: Plot of the tunneling rates against temperature, with comparison to the experimental data. The Initial FCC tunneling rate (fig. 7a) deviates significantly from the experimental measurements, however all other measures provide a close fit. The temperature dependance is significantly different depending on the property measured in the simulation (fig. 7b) although it is unclear which provides the closest fit to the data.

time to equilibrium is an order of magnitude longer however it is clearly a poor measurement of tunneling rate. Activated tunneling rates extrapolated from the high temperature behaviour of fig. 7c have little effect at low temperatures.

4 Simulation Investigation

4.1 Eigenvalue Decomposition

The dynamics of the electron-hydrogen system discussed in section 2 can be investigated by directly simulating the system. This can be done through direct integration of the Schrödinger equation, however if we decompose the initial state into eigenstates of the complete hamiltonian[7]

$$|\Psi(t)\rangle = \exp\left(-i\frac{Ht}{\hbar}\right)\sum_n C_n |n\rangle \tag{62}$$

$$= \sum_n C_n \exp\left(-i\frac{E_n t}{\hbar}\right)|n\rangle \tag{63}$$

we can propagate by multiplying each eigenstate by a phase-factor.

Since we are dealing with a large number of eigenstates it is important to think about both the storage and computational complexity of the two methods (table 3).

Cost	Integration	Decomposition
Time	$\mathcal{O}(n^2 t)$	$\mathcal{O}(n^3 + nd)$
Storage	$\mathcal{O}(nd)$	$\mathcal{O}(n^2 + nd)$

Table 3: Complexity associated with the two methods of solving Schrödinger equation, for n eigenstates, t timesteps and d datapoints. The method of eigenvalue decomposition prevents the $\mathcal{O}(t)$ dependence seen in direct integration by first decomposing the eigenstate ($\mathcal{O}(n^3)$) before multiplying by the relevant phase ($\mathcal{O}(nd)$).

As we are only interested in the evolution of the eigenstates at times much greater than the frequency $\omega = \frac{E}{\hbar}$ integration was found to be much slower than eigenvalue decomposition. One issue is the increased storage cost associated with storing the complete hamiltonian. This could be prevented by working with a sparse matrix, however in practise this was not required.

Although the decomposition is expensive it was only repeated once, allowing us to gather a large number of times at very little additional cost. It was also possible to use the fact that the matrix was hermitian to provide and additional increase in speed.

4.2 Matrix Representation

Working in the unperturbed electron basis (section 2.1) we label each eigenstate according to the index of the hydrogen site and the configuration of the electron system. For n electron states and m hydrogen states there are $m2^n$ eigenstates, however we work with a fixed number of electrons N such that the number of states scales as $m \times \binom{n}{N}$. In practise we were able to simulate a system with ~ 3500 eigenstates, or 14 half filled electron states (table 4). Exchange statistics

Number of States	All Configurations	Half Filled	2 electrons
10	1024	252	45
12	4096	924	66
14	16384	3432	91
16	65536	12870	120

Table 4: Number of eigenstates in the electron-hydrogen system. We were able to simulate a larger number of states using a fixed number of electrons. This method scales particularly well for a system with a low number of electrons.

are important when working with fermions. For self consistency we work in a basis such that electrons with lower energy are always added first. Terms in the hamiltonian pick up a minus sign when there is an odd number of exchanges.

$$a_1^\dagger a_2 \left|2,3\right\rangle = \left|1,3\right\rangle \tag{64}$$

$$a_1^\dagger a_3 \left|2,3\right\rangle = -\left|1,2\right\rangle \tag{65}$$

4.3 Choosing the Initial States

4.3.1 Distribution Of Energies

The electron energies were initially evenly spaced however this lead to rabi oscillations at a fixed frequency. To allow for cancellation of the noise a random offset was introduced into the energy distribution which changed the rabi frequencies between each run.

The electron energy spacing also sets the effective volume of the nickel lattice. The density of states of a free electron gas $g(E)$ is given by [13]

$$g(E) = \frac{V}{2\pi^2}(\frac{2m}{\hbar^2})^{\frac{3}{2}} E^{\frac{1}{2}} \tag{66}$$

We invert this expression to find the implied volume

$$V = 2\pi^2 \frac{g(E)}{E^{\frac{1}{2}}}(\frac{\hbar^2}{2m})^{\frac{3}{2}} \tag{67}$$

At large k we find $g(E)$ is roughly constant so we make the approximation

$$g(E) = \frac{dN}{dE} \sim \frac{1}{E_{space}} \tag{68}$$

where E_{space} is the energy spacing of the simulation. From eq. (28) we find

$$\hat{H}_{int} \propto \frac{1}{V} \propto E_{space} \tag{69}$$

for smaller energy spacing we have a larger volume, and a smaller perturbation.

4.3.2 Distribution Of Electrons

To average over successive simulations we setup the simulation with a random choice of initial states. We can start the hydrogen in the FCC site by setting the amplitudes of the HCP sites to zero before choosing the FCC aptitudes according to a normal distribution.

For a real system at a fixed temperature the electron occupation should follow the fermi-dirac distribution. To match this distribution we set the average amplitude of each state C_k to the square-root of the boltzmann probability P_k.

$$P_k = \exp(-\beta E_k) \tag{70}$$

$$C_k = \exp(-\beta E_k/2) \tag{71}$$

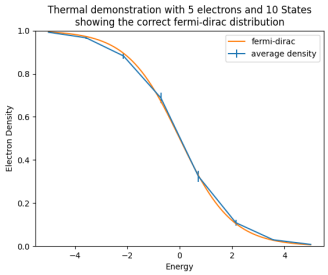

(a) 5 Electrons 10 States

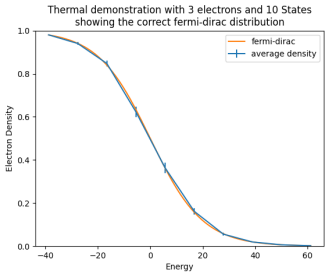

(b) 3 Electrons 10 States

Figure 8: Plot of the electron distribution of a random system. The correct fermi-dirac distribution is seen in both the on and off center systems. Errors are given by the standard deviation of the electron densities, and are therefore larger around the fermi surface where fluctuations are large.

Plotting the electron occupation for fixed N we recover the fermi-dirac distribution (fig. 8). If we were to include a large interaction term, such as those required for the real nickel system the fermi-dirac distribution is no longer seen as this approach does not account for the shift in the perturbed energies (fig. 9). To overcome this limitation the simulation was repeated for small energy bands

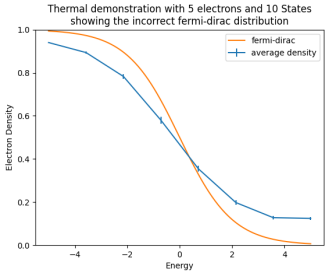

(a) Large interaction

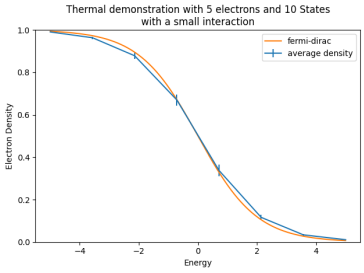

(b) Reduced Interaction

Figure 9: Plot of the fermi-dirac distribution with the inclusion of the full interaction. The correct distribution is only recovered when the interaction is reduced by a factor of 10 (fig. 9b).

(section 4.5) for which the electron distribution was uniform.

4.4 Initial Investigation

To estimate the tunneling rate the system was setup with electrons evenly spaced in $E_k = E_f \pm 2k_bT$. The hydrogen occupation could then be inferred by summing the occupation of electrons in both the FCC and HCP sites. The size of the interaction ($6.21 \times 10^{-21}J$ diagonal, $2.73 \times 10^{-23}J$ off diagonal) was similar to

the separation of electron energies ($9.2\times10^{-22}J$), and as such the approximation required for a fermi-dirac distribution did not hold. For degenerate hydrogen energies (fig. 10) we see tunneling in $10^{-9}s$ however once the hydrogen energy was included we no longer see any tunneling (fig. 11).

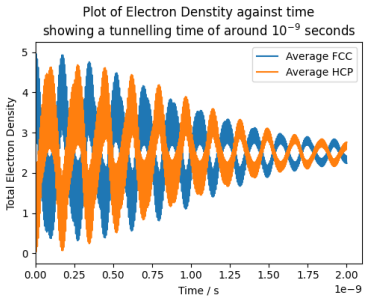

(a) Tunnelling excluding hydrogen energy

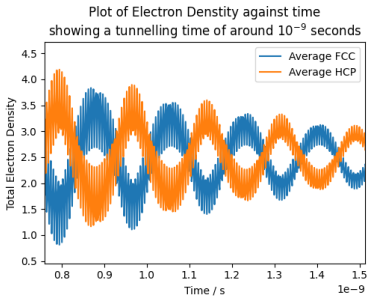

(b) Rapid oscillation of the hydrogen occupation

Figure 10: Plot of the tunnelling rate taken using a simple choice of electron energies, taken evenly in the range $E = E_f \pm 2k_bT$. Simulation with a degenerate hydrogen (fig. 10a) shows tunnelling in around $10^{-9}s$.

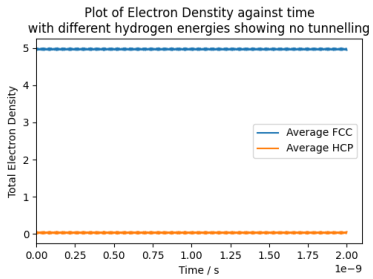

(a) Tunnelling including hydrogen energy

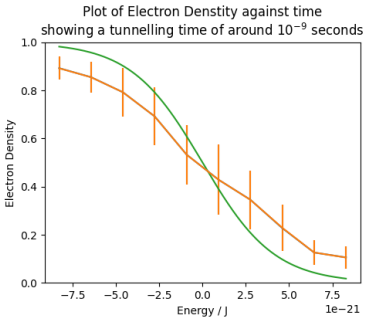

(b) Electron Distribution

Figure 11: Plot demonstrating the issues with the simple approach used to calculate the rate. When including the hydrogen energies (fig. 11a) no tunnelling can be seen, even at much larger timescales. Even without the inclusion of hydrogen energies the incorrect electron distribution is seen (fig. 11b).

4.5 Small Band Approach

To limit the effect of the incorrect fermi distribution we take electrons with a similar occupation localised in a small region of the fermi surface.

One issue is that states at the edge of the band will be 'missing' states to mix with during the perturbation. We can approximate this overlap using first

order perturbation theory.

$$|n\rangle = |n^{(0)}\rangle + \sum_{K \neq n} \frac{\langle k^{(0)}| \hat{H}_{int} |n^{(0)}\rangle}{E_n^{(0)} - E_k^{(0)}} |k^{(0)}\rangle \tag{72}$$

Since $\hat{H}_{int} \propto E_{space}$ (eq. (69)) the overlap between neighbours does not depend on the energy spacing. Luckily the interaction is small enough such that states only interact with their closest neighbours (fig. 12), and the effect of these missing states should be small. Tunneling could also be influenced through

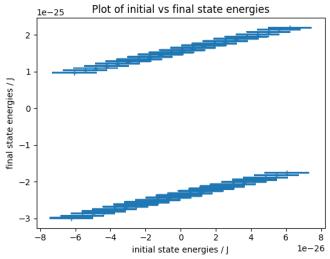

(a) Final State Energies

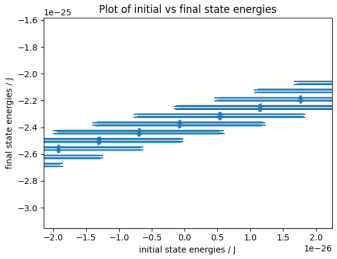

(b) Detailed view of lower energies

Figure 12: Average initial state energy weighted by the occupation probability. The final state energy is separated into symmetric and antisymmetric contributions (fig. 12a). In fig. 12b we can see each state is highly degenerate, and mixing is limited to the four nearest neighbours.

a combination of several electron 'hops'. Due to the energy time uncertainty principle $\Delta E \Delta T \geq \frac{\hbar}{2}$ we expect the total energy to be conserved to within

$$\Delta E \sim \frac{\hbar}{2\Delta t} \tag{73}$$

so that for a tunnelling time of $\sim 10^{-9}s$ we expect an energy fluctuation of $\sim 5 \times 10^{-26} J$. We therefore choose states separated by at-least $10^{-25} J$. Interaction with states outside the band is then prohibited through energy conservation.

4.6 Different Hydrogen Energy

If we add the hydrogen energies to the simulation we no longer see tunnelling on any timescale. Repeating the analysis in section 4.5 we see that eigenstate mixing is dominated by eigenstates degenerate in energy. In the initial approach we miss much of the overlap which could contribute to tunnelling. To ensure that we always have states degenerate in energy we introduce two electron bands separated by the hydrogen energy difference. With this approach we find the final-state energies are split into three bands which are separated into distinct groups. To promote mixing between these each group we increase the width of each band, however different mixing within each band leads to a reduction in the

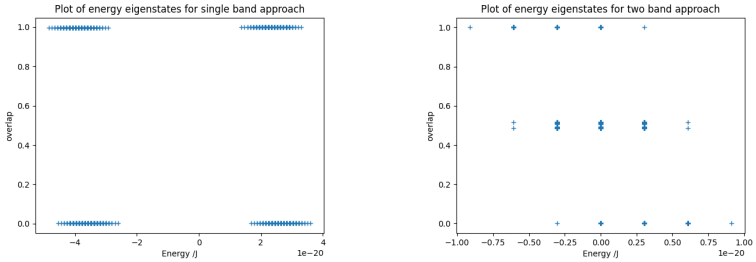

(a) One Band Overlaps (b) Two Band Overlaps

Figure 13: Plot of eigenstate energies against the FCC 'occupation-fraction' For a single band we see very little overlap between the FCC and HCP states (fig. 13a) as the energies are poorly matched. Introducing two bands separated by the hydrogen energy difference (fig. 13b) we find mixing between states which are degenerate in energy

overlap. To prevent this we simply remove the diagonal interaction, however in (section 5.6) we find this changes the measured tunneling rate. Given the rate scales as $N(1-N')$ it is possible to calculate a theoretical equilibrium, however it does not tend to this value even when working with a small band. We do however see a reduction in fluctuations if the system is initially prepared with this occupation (fig. 15a). We also find material cools during the tunneling process as energy is transferred from the electron gas to the hydrogen (fig. 15b). The temperature shift can be reduced by adding more electrons to the simulation.

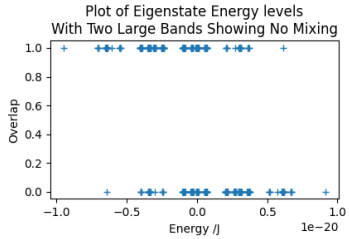

(a) Large Band Mixing

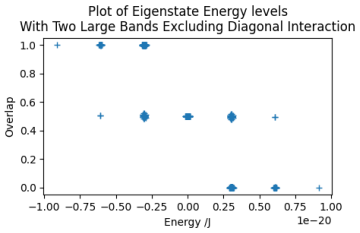

(b) Large Band No Diagonal

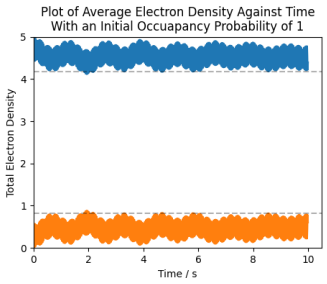

(c) Large Initial Occupation

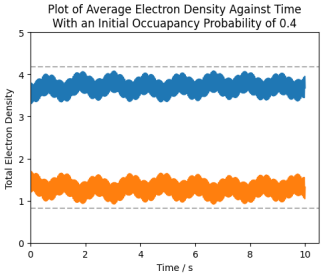

(d) Small Initial Occupation

Figure 14: fig. 14a demonstrates the issue with using a large band; the diagonal interaction causes mixing within groups of eigenstates which lifts the degeneracy required for the off diagonal interaction. This can be fixed by removing the diagonal interaction (fig. 14b) however in section 5.6 we find this is necessary for the correct tunneling behaviour. Even with a small band the predicted equilibrium behaviour is not seen (figs. 14c and 14d). There is therefore very little evidence that this method should be used to model the true electron-hydrogen dynamics.

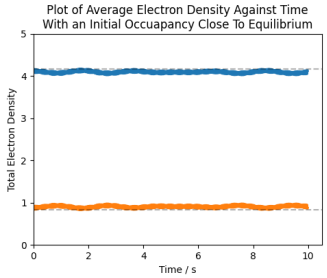

(a) Evoulution Close To Equilibrium

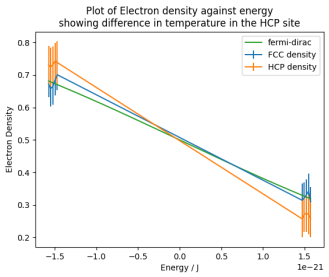

(b) Two Band Electron Distribution

Figure 15: Interesting features of the two band dynamics. In fig. 15a we find noise is reduced when the hydrogen is prepared in a state close to the predicted equilibrium. This suggests it is true equilibrium of the system. In fig. 15b the temperature shift can be seen. This is a consequence of energy transfer between the electron gas to the hydrogen.

5 Simulation Results

As the previous investigation demonstrates it is not possible to directly incorporate the hydrogen energy into the simulation, however we can ignore the difference in energy for the same reason we assume separability of the electron-hydrogen density matrix in section 3.2. The key difference between degenerate and non-degenerate tunneling is the location of the electrons immediately after tunneling. Since mixing only occurs between states degenerate in energy we expect to see a lower energy distribution in the HCP site, however in the limit of a large number of electrons this energy difference is negligible. Since the off diagonal interaction is small we find the individual electrons transition at a much faster rate than hydrogen, and it is reasonable to expect that the exact electron distribution after a transition has no effect on the hydrogen dynamics. The electron distribution during a transition should have an effect on the rate however, as an electron can only transition to a state which is previously empty. The method used to account for this behaviour is discussed in section 5.3.

5.1 Rate at 150K

To calculate the tunneling rate we limit ourselves to degenerate hydrogen, making use of the small band approach discussed in section 4.5 with a bandwidth of $5 \times 10^{-26} J$. The hydrogen occupation was seen to oscillate rapidly inside a wavepacket which was fitted to $\exp(-R^2 t^2)$.

The occupation fraction $N = \frac{n}{s}$ was varied by changing the number of electrons (n) and number of states (s), plotted in fig. 16. The rate was seen to change at constant N as s was increased however the asymptotic behaviour followed a simple form

$$R(N, N) = 4R_0 N(1 - N) \tag{74}$$

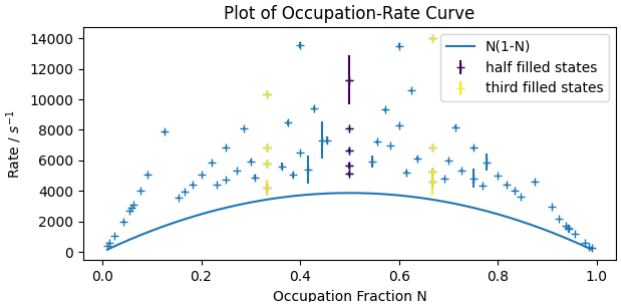

Figure 16: The occupation-rate curve at 150K, with the predicted rate from half filled data. The rate is seen to tend to a constant value as the number of states $s \to \infty$.

where R_0 is a rate constant to be determined. This is exactly the rate curve we see in the Lindblad analysis when hydrogen tunnelling is paired with a single electron transition.

5.2 Calculating R_0

The rate depends only on a single parameter R_0 which we extrapolate from the asymptotic limit of a single occupation fraction. This can only be achieved for $N = \frac{1}{2}$, where by far the largest number of datapoints were collected (fig. 17). As $N \to 0$ we find $R(N, N) \sim 4R_0N = 4R_0(\frac{n}{s})$ which we use to find a second

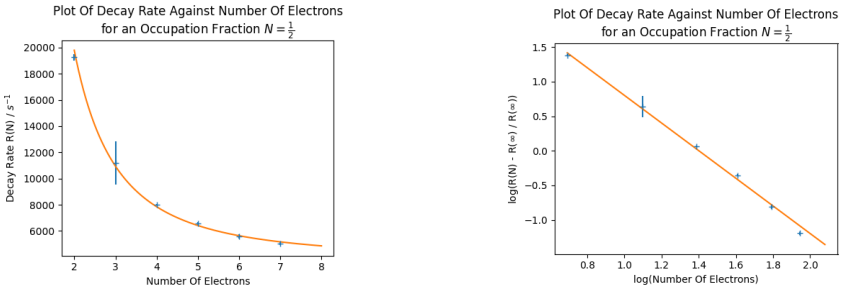

(a) Half Filled Rates

(b) log Half Filled Rates

Figure 17: Decay rates against number of electrons n for $N = 0.5$. The decay rates were fitted to $R(n) = R(\infty) + (\frac{A}{n})^2$ where $R(\infty) = R_0$ was found to be $3900 \pm 100s^{-1}$.

value for R_0. Since the rate curve is symmetric we expect identical behaviour for n electrons and n holes, however since the 1 electron data was inconsistent (fig. 18a) we limit the analysis to 2 electron or 2 hole data. The $N = \frac{1}{2}$ data gave a rate constant $R_0 = 3900 \pm 100s^{-1}$, and for the $n = 2$ data we find $R_0 = 8400 \pm 600s^{-1}$. The decay rate suggested from the $N = 2$ data is unlikely to give an accurate representation of the decay rate, as it predicts an asymptotic rate at $N = 0.5$ well above that measured even for $n = 5$ electrons. Repeating the measurements at several temperatures it was not possible to identify any temperature dependance of the rate constant R_0.

5.3 Corrected Transition Rate

In the real hydrogen system energy is conserved during tunneling, which leads to the electron loosing energy as the hydrogen transitions from FCC to HCP sites (section 4.6). To correct for this behaviour we need to find the tunneling rate from an occupation N to an occupation N'. Due to the arguments outlined in appendix B a general system with a different forward and backward rate the combined tunneling rate is given by

$$R(N, N') = R(N \to N') + R(N' \to N) \tag{75}$$

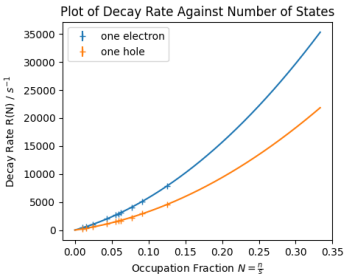

(a) 1 Electron Data

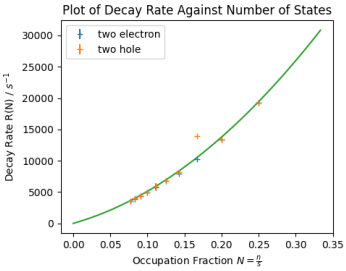

(b) 2 Electron Data

Figure 18: Asymptotic form of the decay rates as $N \to 0$ at a fixed number of electrons n. The single electron and single hole data is inconsistent (fig. 18a). The two electron data was fitted to $R(N) = 4R_0N + AN^2$ to give an overall rate constant $R_0 = 8400 \pm 600s^{-1}$. This is not an accurate representation of the true decay rate, as it predicts a rate at $N = 0.5$ well above that measured even for $n = 5$ electrons.

where $R(N \to N')$, $R(N' \to N)$ are the forward and backwards tunneling rates respectively. There are two obvious ways to modify the tunneling rate

$$R(N \to N') = 2R_0N(1 - N) \tag{76}$$
$$R(N \to N') = 2R_0N(1 - N') \tag{77}$$

all of which have the correct limit in the case $N = N'$, when the forward rate is half of the total rate given by eq. (74)

$$R(N \to N) = 2R_0N(1 - N) \tag{78}$$

eq. (76) assumes the rate only depends on the initial occupation and eq. (77) assumes the rate depends on the probability the initial state is occupied N and the final state is unoccupied $1 - N'$. We could also consider a correction

$$R(N \to N') = 2R_0\sqrt{N(1 - N)N'(1 - N')} \tag{79}$$

which implies a two jump process. The electron falls to a lower band before being promoted back into its original location, with each jump contributing $\sqrt{N(1 - N')}$ to the rate. Note we have ignored functions such as $2R_0N'(1-N')$ which would give the same overall rate as $2R_0N(1 - N)$.

5.4 Total Tunnelling Rate

To recover the total tunneling rate the occupation rate curve is converted into an energy rate using the fermi-dirac distribution. For $R(N \to N') = 2R_0N(1-N')$

we find

$$N(\epsilon) = \frac{1}{1+\exp\left(\beta(\epsilon-\mu)\right)} \tag{80}$$

$$R(\epsilon \to \epsilon') = 2R_0 \frac{1}{1+\exp\left(\beta(\epsilon-\mu)\right)}\left(1 - \frac{1}{1+\exp\left(\beta(\epsilon'-\mu)\right)}\right) \tag{81}$$

$$= 2R_0 \frac{\exp\left(\beta(\epsilon'-\mu)\right)}{(1+\exp\left(\beta(\epsilon-\mu)\right))(1+\exp\left(\beta(\epsilon'-\mu)\right))} \tag{82}$$

where we have assumed uniform occupation within a band. The rate curve (fig. 19) can then be integrated to give an overall tunneling rate. Similarly to the Lindblad analysis we multiply the rate by a factor of 3 for neighbouring sites and 2 for spin. Further investigation into the effect of spin supports this, however direct calculation of R was not possible due to the increased number of states required. The results of this analysis are given in table 5.

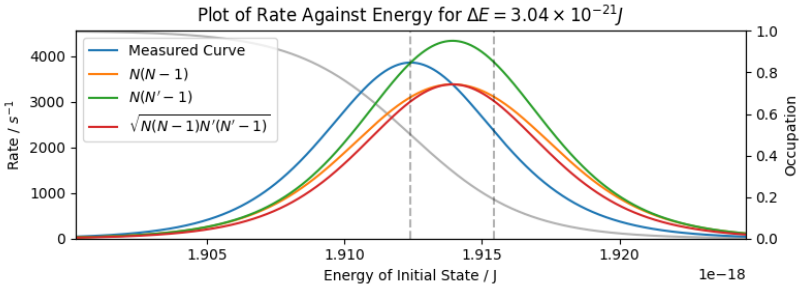

Figure 19: Plot of the corrected tunneling rate curve against energy. As the occupation curve (shown in grey) falls to 0 the rate falls also. The corrected rate is seen to peak at half of the hydrogen energy difference above the fermi energy (grey dashed line).

Rate	$\frac{1}{2}$ Filled $10^9 s^{-1}$	2 Electron $10^9 s^{-1}$
Uncorrected	3.6 ± 0.1	7.9 ± 0.6
$N(1-N)$	3.6 ± 0.1	7.87 ± 0.6
$N(1-N')$	4.3 ± 0.1	9.24 ± 0.7
$\sqrt{N(1-N)N'(1-N')}$	3.3 ± 0.1	7.20 ± 0.6

Table 5: Comparison of decay rates at 150K. The tunneling rates taken from the $\frac{1}{2}$ filled data is close to the experimental rate of $3.3 \times 10^9 s^{-1}$. As discussed in section 5.2 the two electron decay represent a large overestimate of the true tunneling rate.

5.5 Investigating Rate Corrections

Given the calculated tunneling rates it is possible to compare the temperature dependence with experiment. As no temperature dependence could be seen in the simulation we use the same rate constant calculated at $150K$ at all temperatures. The temperature dependence seen in fig. 20 is therefore entirely due to the corrections made in section 5.3. Outside the experimentally relevant range

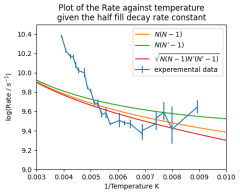

(a) Half Filled Data

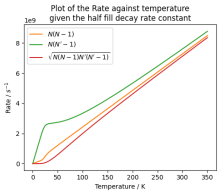

(b) Large Temperature Range

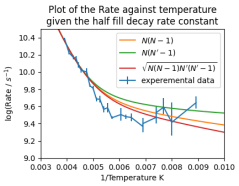

(c) Including Activated Tunneling

Figure 20: Plot of the decay rates against temperature with a comparison to experiment. The half filled data provided a good fit to the experimental tunneling rates (fig. 20a). The three methods of correcting the rate introduced in section 5.3 gave a similar temperature dependence, all of which were consistent with experimental data. In the high temperature limit fig. 20b the tunneling rate is seen to converge as $N \to N'$. The rates are seen to diverge at $25K$ however this is well below the range of temperatures measured in experiment.

we see that the tunneling rates remain similar at all temperatures (fig. 20b). Although we have no way to predict the behaviour at such low temperatures, the choice $\sqrt{N(1-N)N'(1-N')}$ exhibits much smoother behaviour as $T \to 0$. With comparison to the Lindblad equation however (section 6.1) the $N(1-N')$ correction seems to be the most physically justifiable.

5.6 Tunneling Without Self Interaction

In section 4.6 the diagonal interaction prevented mixing of the FCC and HCP sites once hydrogen energy was introduced. It is therefore useful to investigate the extent to which this interaction effects the interaction (fig. 21). The data gave a rate constant of $R_0 \sim 13000s^{-1}$, more than $3\times$ that of the full interaction. It is clear that this self interaction has an important role in the simulated tunneling rate, and removing such an interaction is not a valid approach to calculate a non-degenerate tunneling rate.

6 Further Work

Given the results of direct simulation it is possible to examine the approximations used to arrive at the Lindblad equation.

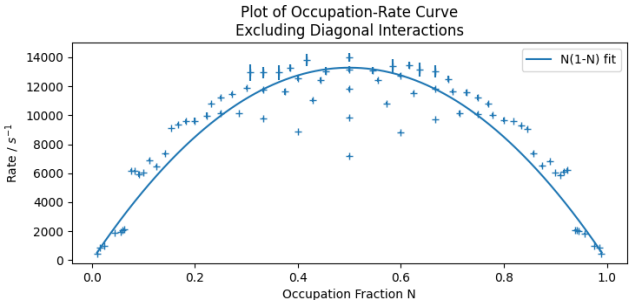

Figure 21: Decay rates measured without the inclusion of diagonal interaction. We see a much larger rate constant ($R_0 \sim 13000 s^{-1}$), and the rates are seen to increase (rather than decrease) as $n \to \infty$.

6.1 Single State Tunnelling Rate

When simulating the degenerate hydrogen tunneling in section 5.1 we found that the tunneling rate grew proportional to $4R_0N(1-N)$. This corresponds exactly to the form of the integrand of eq. (51), which was proportional to $N_1(1-N_3)$ where $E_{k3} = E_{k1} + \omega$, and ω is equal to the difference in hydrogen energies

$$\Gamma_{i,j,k,l}(\omega) = 4 \int \frac{d^3\mathbf{k}_1}{(2\pi)^3} \frac{d^3\mathbf{k}_3}{(2\pi)^3} V_{i,j} V_{k,l} N_1 (1 - N_3) \frac{m\delta(k_3 \pm \sqrt{k_1^2 + 2m\omega})}{\sqrt{k_1^2 - 2m\omega}} \tag{83}$$

This suggests that the process is dominated by single electron transitions, an assumption that was made in eq. (37) when expanding the equation of motion to second order.

If we were to look at the tunneling for $\omega \neq 0$ we find that the correct way to modify the tunneling rate in the simulation should be to set $R(N \to N') = 2R_0N(1-N')$ corresponding to eq. (77) in section 5.3.

6.2 Final State Correction

In section 5 we argued that the electron state immediately after a transition should not effect the dynamics of the system, however in the Lindblad analysis it should be possible to properly take into account the change in electron distributions through the introducing a coupling between the electron and hydrogen density matrices. Although this a difficult problem in general if we were to introduce a coupling

$$\hat{\rho}_t = \sum_{m,n} \hat{\rho}_{m,n} \otimes (\hat{\rho}_E)_{m,n} \tag{84}$$

we can follow the same procedure as in section 3.2 to arrive at a modified redfield equation

$$\langle m|\,\dot{\hat{\rho}}(t)\,|n\rangle = \sum_{i,j,k,l} \exp\left(-i(\omega_{i,j}-\omega_{k,l})t\right)\Gamma^{m,n}_{i,j;k,l}(\omega_{k,l})[S_{k,l}\hat{\rho}(t)_{m,n}, S^{\dagger}_{i,j}] \quad (85)$$
$$+\exp\left(i(\omega_{i,j}-\omega_{k,l})\right)\Gamma^{*\,m,n}_{k,l;i,j}(\omega_{i,j})[S_{k,l}, \hat{\rho}(t)_{m,n}S^{\dagger}_{i,j}]$$

where

$$\Gamma^{m,n}_{i,j,k,l}(\omega) = \int_0^{\infty} ds \exp\left(i\omega s\right) Tr_E[E^{\dagger}_{i,j}(t)E_{k,l}(t-s)(\hat{\rho}_E)_{m,n}] \quad (86)$$

The problem is then how best to express both the statistical and quantum uncertainty in the form of a density matrix.

6.3 Rotating Wave Approximation

If we relax the rotating wave approximation made in section 3.3 we arrive at the full Redfield equation (appendix C.2).

$$\langle m|\,\dot{\hat{\rho}}(t)\,|n\rangle = \sum_{i,j} \exp\left(-i\Delta E_{n,j;m,i}t\right)\Gamma_{n,j;m,i}(\omega_{m,i})\rho_{i,j} \quad (87)$$
$$-\exp\left(-i\Delta E_{i,m;i,j}t\right)\Gamma_{i,m;i,j}(\omega_{i,j})\rho_{j,n}$$
$$+\exp\left(i\Delta E_{n,j;m,i}t\right)\Gamma_{n,j;m,i}(\omega_{n,j})\rho_{i,j}$$
$$-\exp\left(i\Delta E_{i,j;i,n}t\right)\Gamma_{i,j;i,n}(\omega_{i,j})\rho_{m,j}$$

This equation produces extra oscillations on top of the Lindblad result, with a characteristic timescales of $\frac{2\pi}{\omega_{1,0}} = 2.13 \times 10^{-13}s$. Plotting the full solution (fig. 22) we see exactly the same behaviour as that predicted by the Lindblad result. In theory we should also be able to solve the redfield equation for multiple hydrogen sites, however the additional computational complexity rules this out. It is possible to approximate the behaviour seen in the many site model by placing a sink at the HCP site (fig. 22c). In this case we again see good agreement with the Lindblad equation.

6.4 Separable Density matrix

In the analysis of the Lindblad equation we also assumed that is was possible to factorise the density matrix

$$\hat{\rho}_t(t) = \hat{\rho}(t) \otimes \hat{\rho}_E(0) \quad (88)$$

It is clear from the initial and final state energy distribution that in the limit of a large number of states the diagonal elements are completely uncorrelated with the hydrogen occupation. In the real simulation the electron density matrix is not diagonal, however if we average over a small period of time the average is seen to fall to zero (fig. 23). The approximation therefore holds for the same

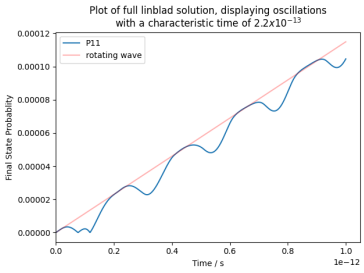

(a) Complete solution for small times

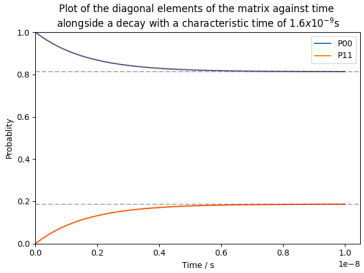

(b) Complete solution for long times

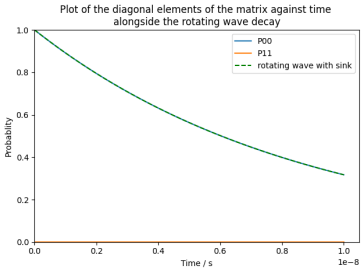

(c) Complete solution with sink

Figure 22: Plot of the full solution of the Redfield equation. On short timescales (fig. 22a) the solution is seen to oscillate with a characteristic frequency of 2.1×10^{-13}s however at long timescales (fig. 22b) the solution decays at the same rate as the Lindblad equation. The solution is also well behaved with the inclusion of a sink at the HCP site (fig. 22c).

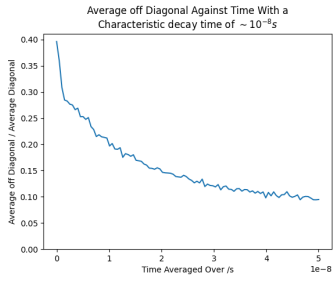

(a) Average Off-Diagonal Decay

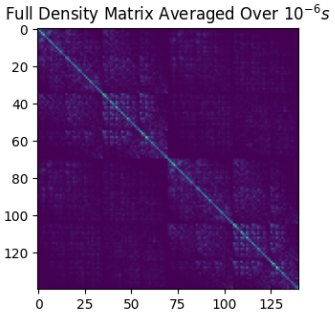

(b) Averaged Density Matrix

Figure 23: Plot of the average electron density matrix for a system of 5 electrons and 10 states corresponding to a tunneling time of $\sim 2 \times 10^{-4}s$. The average off diagonal elements can be seen to fall in around $\sim 2 \times 10^{-8}s$.

reason we are able to ignore the off-diagonal terms in the hydrogen density matrix (section 6.3). Since the off diagonal terms oscillate at much shorter timescales they have no effect on the dynamics of the system.

6.5 q Dependance

For this report we use a q-independent model of the electron hydrogen interaction. If we instead include the full form of the interaction potential into eq. (51) we find a Lindblad rate constant that is $0.418 \times$ that previously calculated.

We also expect a contribution from the $\mathbf{q}$ dependance of the hydrogen overlap fourier transform, however it is unclear how best to interpret the discrete DFT analysis as a continuous function of $\mathbf{q}$.

For the simulation it will always be necessary to assume a $\mathbf{q}$-independent matrix element in general, as it is not possible to include enough states to properly sample all possible initial and final states in 3D. The corrections made in the Lindblad analysis could be applied to the simulation, producing an effective matrix element depending only on the energy difference between two states.

6.6 Realistic Treatment of Electrons

In the development of the electron-hydrogen model we also assumed an ideal electron gas, with a fermi energy of $1.91 \times 10^{-18} J$. The real fermi energy of nickel actually slightly lower, at only $1.24 \times 10^{-18} J$, possibly since the two valence electrons are not fully delocalised. The fermi surface of nickel is also not entirely spherical [5], indeed it is different for each spin. This is the cause of ferromagnetic properties within the metal [23].

This behaviour could be included in the Lindblad analysis through a modification of eq. (51), however it is not possible to incorporate any non-spherical behaviour into the simulation without the introduction of an effective constant. The complex nature of the nickel band-structure means that this could favour low or high $\mathbf{q}$ scattering, which would lead to either an increase or decrease in the overall rate. The hope is that the surface is sufficiently 'smoothed out' by excitations at high temperature such that this is only a small correction.

6.7 Other Sources of Decoherence

It is possible that decoherence is also introduced to the hydrogen through other interactions within the material, such as the thermal motion of nickel atoms. This would lead to an increased hopping rate.

7 Conclusion

A simple model of an electron-hydrogen system on Ni was developed to explain the incoherent tunneling of hydrogen on a Ni(111) surface.

Through an application of the Lindblad equation a simple, closed form expression for the hydrogen density matrix evolution was found, which was used to find an expression for the rate at which the combined FCC occupation reached equilibrium

$$R = 12\cosh\left(\frac{\beta\omega_{k,l}}{2}\right)\mathcal{C}_{1,0}\mathcal{C}_{0,1}\sqrt{\pi}\frac{32k_f^2\epsilon_0^2\hbar^3}{\beta e^4 m_e^2} \tag{89}$$

where $\omega_{i,j} = E_i - E_j$, E_i is the energy at site i, $\mathcal{C}_{i,j}$ is the hydrogen overlap fraction. Rates extracted from the combined FCC occupation ($1.8 \times 10^{-9}s^{-1}$) next HCP occupation ($2.3 \times 10^{-9}s^{-1}$) next FCC occupation ($1.5 \times 10^{9}s^{-1}$) and initial FCC occupation ($2.5 \times 10^{9}s^{-1}$) were all close to the experimental rate of $3.3 \times 10^{9}s^{-1}$ at 150K[24]. The mean squared distance was also shown to increase linearly with time, as expected from a decoherent stochastic process. From this a tunneling rate of $2 \times 10^{9}s^{-1}$ was extracted, which was also constant with the data at 150K.

The behaviour of the full electron-hydrogen model was then investigated through direct integration of the Schrödinger equation. It was found that a simulation including the energy of hydrogen was not possible, and instead a model of degenerate hydrogen was used to measure the tunneling rates. This model predicted a tunneling rate of $3.6 \pm 0.1 \times 10^{9}s^{-1}$ at $150K$ which gave a good prediction of the experimental value of $3.3 \times 10^{9}s^{-1}$[24]. A corrected tunneling rate made with comparison to the Lindblad equation was however slightly higher at $4.3 \pm 0.1 \times 10^{9}s^{-1}$. The corrected rate was shown to have a temperature dependance consistent with that seen in experiment within the incoherent regime.

Results of the simulation were applied to assess some of the approximations made in the Lindblad equation. The simulation provided evidence that the second order approximation used in the Lindblad analysis was correct, as both methods found a rate proportional to $N(1-N')$. It was also argued that the off-diagonal elements of the electron density matrix had no effect on the tunneling rate.

To test this model further it should also be possible to apply the same techniques to predict the ground state to ground state tunneling of deuterium, however there is currently discussion surrounding the accuracy of the experimental data. The results could also be used to investigate the H-Ru(111) and D-Ru(111) however the fermi surface of Ruthenium is much less spherical and hence the free electron approximation may no longer hold.

To provide more precise predictions of the tunneling rate it will be necessary to investigate the extent to which q-dependance of both the interaction and the hydrogen overlap effects the model. It is thought that this could cause a significant reduction in the calculated tunneling rate. It may also be necessary to investigate other sources of decoherence within the material.

References

[1] Dr R Batley. *Advanced Quantum Physics Examples Sheet 2*. Oct. 2019.

[2] Heinz-Peter Breuer and Francesco Petruccione. *The Theory of Open Quantum Systems*. Jan. 2006, p. 117.

[3] A.O Caldeira and A.J Leggett. "Quantum tunnelling in a dissipative system". In: *Annals of Physics* 149.2 (1983), pp. 374–456.

[4] G. X. Cao, E. Nabighian, and X. D. Zhu. "Diffusion of Hydrogen on Ni(111)". In: *Physical Review Letters* 79.19 (1997), pp. 3696–3699.

[5] T. S. Choy et al. *A database of fermi surface in virtual reality modeling language (vrml)*. 2000. URL: `http://www.phys.ufl.edu/fermisurface/` (visited on 03/31/2021).

[6] Dariusz Chruściński and Saverio Pascazio. "A Brief History of the GKLS Equation". In: *Open Systems and Information Dynamics* 24.03 (Sept. 2017).

[7] G. Conduit. Private communication. Dec. 2020.

[8] Wheeler P. Davey. "Precision Measurements of the Lattice Constants of Twelve Common Metals". In: *Phys. Rev.* 25 (6 June 1925), pp. 753–761.

[9] H. Ehrenreich, H. R. Philipp, and D. J. Olechna. "Optical Properties and Fermi Surface of Nickel". In: *Phys. Rev.* 131 (6 Sept. 1963), pp. 2469–2477.

[10] Vittorio Gorini, Andrzej Kossakowski, and E. C. G. Sudarshan. "Completely positive dynamical semigroups of N-level systems". In: *Journal of Mathematical Physics* 17.5 (1976), pp. 821–825.

[11] David J. Griffiths and Darrell F. Schroeter. "Quantum Mechanics in Three Dimensions". In: *Introduction to Quantum Mechanics*. 3rd ed. Cambridge University Press, 2018, pp. 147–148.

[12] A.P. Jardine et al. "Helium-3 spin-echo: Principles and application to dynamics at surfaces". In: *Progress in Surface Science* 84 (Nov. 2009), pp. 323–379.

[13] Charles Kittel. "Introduction to solid state physics." eng. In: New York: Wiley, 1953. Chap. 12, p. 228.

[14] Willis E. Lamb. "Theory of an Optical Master". In: *Phys. Rev.* 134 (6A June 1964), pp. 1429–1450.

[15] Austen Lamcraft. *Theoretical Physics 2, Topics In Quantum Theory Lecture Notes*. Jan. 2019.

[16] T.-S. Lin and R. Gomer. "Diffusion of 1H and 2H on the Ni(111) and (100) planes". In: *Surface Science* 255.1 (1991), pp. 41–60.

[17] G. Lindblad. "On the generators of quantum dynamical semigroups". In: *Communications in Mathematical Physics* 48.2 (June 1976), pp. 119–130.

[18] Daniel Manzano. "A short introduction to the Lindblad master equation". In: *AIP Advances* 10.2 (Feb. 2020).

[19] Yuli V. Nazarov and Jeroen Danon. “Second quantization”. In: *Advanced Quantum Mechanics: A Practical Guide*. Cambridge University Press, 2013, pp. 63–86.

[20] A.G. Redfield. “The Theory of Relaxation Processes”. In: *Advances in Magnetic Resonance*. Ed. by John S. Waugh. Vol. 1. Advances in Magnetic and Optical Resonance. Academic Press, 1965, pp. 1–32.

[21] S. Saito et al. “Incoherent and Coherent Tunneling of Macroscopic Phase in Flux Qubits”. In: *Quantum Computing and Quantum Bits in Mesoscopic Systems*. Ed. by A. J. Leggett, B. Ruggiero, and P. Silvestrini. Boston, MA: Springer US, 2004, pp. 161–169.

[22] J. J. Sakurai and Jim Napolitano. “Modern Quantum Mechanics”. In: 3rd ed. Cambridge University Press, 2020. Chap. 3, pp. 174–175.

[23] J. C. Slater. “The Ferromagnetism of Nickel”. In: *Phys. Rev.* 49 (7 May 1936), pp. 537–545.

[24] Jianding Zhu. “Study of quantum effects in adsorbate diffusion”. PhD thesis. Churchill College, University of Cambridge, Apr. 2015.

A Calculating The Potential

The potential of hydrogen in the position basis can be found making use of the greens function of the coulomb potential[1]

$$V(\mathbf{r}) = \frac{e^2}{4\pi\epsilon_0}(-\frac{1}{r} + \int \frac{|\psi(\mathbf{r})|^2}{|\mathbf{r}-\mathbf{r}'|}d\mathbf{r}') \tag{90}$$

when we assume the electron lies in the 1s state[11]

$$\psi(\mathbf{r}) = (\pi a_0^3)^{\frac{1}{2}} e^{-\frac{r}{a_0}} \tag{91}$$

we arrive at the following potential

$$V(\mathbf{r}) = \frac{e^2}{4\pi\epsilon_0}(-\frac{1}{r} + \pi a_0^3 \int \frac{e^{-\frac{2r}{a_0}}}{|\mathbf{r}-\mathbf{r}'|}d\mathbf{r}') \tag{92}$$

If we make use of two standard results

$$\int \frac{1}{r} e^{i\mathbf{q}.\mathbf{r}} d^3\mathbf{r} = \frac{4\pi}{q^2} \tag{93}$$

$$\int e^{-\alpha r} e^{i\mathbf{q}.\mathbf{r}} d^3\mathbf{r} = \frac{8\pi\alpha}{(\alpha^2+q^2)^2} \tag{94}$$

$$\tag{95}$$

with $\alpha = \frac{2}{a_0}$ we end up with

$$V(\mathbf{q}) = \frac{e^2}{4\pi\epsilon_0}(-\frac{4\pi}{q^2} + \frac{\pi a_0^3}{q^2}\frac{8\pi\alpha}{(\alpha^2+q^2)^2}) \tag{96}$$

$$= \frac{e^2}{\epsilon_0 q^2}(\frac{\alpha^4}{(\alpha^2+q^2)^2} - 1) \tag{97}$$

$$= -\frac{e^2}{\epsilon_0}\frac{2\alpha^2+q^2}{(\alpha^2+q^2)^2} \tag{98}$$

B Combined Tunnelling Rates

Suppose we have a system with two states x_1, x_2 with a forward and backwards tunnelling rate γ_1, γ_2. We can express the equations of motion in matrix form

$$\begin{pmatrix} \dot{x}_1 \\ \dot{x}_2 \end{pmatrix} = \begin{pmatrix} -\gamma_1 & \gamma_2 \\ \gamma_1 & -\gamma_2 \end{pmatrix} \begin{pmatrix} x_1 \\ x_2 \end{pmatrix} \tag{99}$$

from here we find the eigenvalues and eigenvectors of the matrix.

$$\lambda_1 = -\gamma_1 - \gamma_2 \Rightarrow V_1 = a \begin{pmatrix} 1 \\ -1 \end{pmatrix} \tag{100}$$

$$\lambda_2 = 0 \qquad \Rightarrow V_1 = a \begin{pmatrix} \frac{\gamma_2}{\gamma_1} \\ 1 \end{pmatrix} \tag{101}$$

Given a state initially in 1 we can decompose it into these eigenstates to find the behaviour at a later time

$$\begin{pmatrix} x_1(0) \\ x_2(0) \end{pmatrix} = \begin{pmatrix} 1 \\ 0 \end{pmatrix} \tag{102}$$

$$= \frac{1}{1+\frac{\gamma_2}{\gamma_1}}(\begin{pmatrix} \frac{\gamma_2}{\gamma_1} \\ 1 \end{pmatrix} + \begin{pmatrix} 1 \\ -1 \end{pmatrix}) \tag{103}$$

$$\Rightarrow \begin{pmatrix} x_1(t) \\ x_2(t) \end{pmatrix} = \frac{1}{1+\frac{\gamma_2}{\gamma_1}}(\begin{pmatrix} \frac{\gamma_2}{\gamma_1} \\ 1 \end{pmatrix} + \begin{pmatrix} 1 \\ -1 \end{pmatrix} \exp\left(-(\gamma_1+\gamma_2)t\right)) \tag{104}$$

The system therefore decays at a rate proportional to $\gamma_1 + \gamma_2$ and reaches an equilibrium at

$$\begin{pmatrix} x_1(\infty) \\ x_2(\infty) \end{pmatrix} = \frac{1}{\gamma_1+\gamma_2}\begin{pmatrix} \gamma_2 \\ \gamma_1 \end{pmatrix} \tag{105}$$

C From Redfield to the Lindblad Equation

Starting from the expression for $\dot{\rho}(t)$ in section 3.2

$$\dot{\hat{\rho}}(t) = \sum_{i,j,k,l} \exp\left(-i(\omega_{i,j}-\omega_{k,l})t\right)\Gamma_{i,j;k,l}(\omega_{k,l})[S_{k,l}\hat{\rho}(t), S_{i,j}^\dagger] \tag{106}$$
$$+ \exp\left(i(\omega_{i,j}-\omega_{k,l})\right)\Gamma^*_{k,l;i,j}(\omega_{i,j})[S_{k,l}, \hat{\rho}(t)S_{i,j}^\dagger]$$

where $S_{i,j} = \hat{a}_i^\dagger \hat{a}_j$, $\omega_{i,j} = E_i - E_j$, the energy of the hydrogen atoms excluding the interaction, and Γ is the Lindblad rate constant defined in eq. (43). To make the following calculation easier we deal with a single component of ρ

$$\langle m|\,\dot{\hat{\rho}}(t)\,|n\rangle = \sum_{i,j,k,l} \exp\left(-i\Delta E t\right)\Gamma_{i,j;k,l}(\omega_{k,l})\,\langle m|\,[S_{k,l}\hat{\rho}(t), S_{i,j}^\dagger]\,|n\rangle \tag{107}$$
$$+ \exp\left(i\Delta E t\right)\Gamma^*_{k,l;i,j}(\omega_{i,j})\,\langle m|\,[S_{k,l}, \hat{\rho}(t)S_{i,j}^\dagger]\,|n\rangle$$

where $\Delta E = \omega_{i,j} - \omega_{k,l}$. Focusing on the commutators we have

$$\langle m|\,[S_{k,l}\hat{\rho}(t), S_{i,j}^\dagger]\,|n\rangle = \sum_{\alpha,\beta}\rho_{\alpha,\beta}\,\langle m|\,[\hat{a}_k^\dagger\hat{a}_l\hat{a}_\alpha^\dagger\hat{a}_\beta, \hat{a}_j^\dagger\hat{a}_i]\,|n\rangle \tag{108}$$

$$= \sum_{\alpha,\beta}\rho_{\alpha,\beta}\,\langle m|\,\hat{a}_k^\dagger\hat{a}_l\hat{a}_\alpha^\dagger\hat{a}_\beta\hat{a}_j^\dagger\hat{a}_i - \hat{a}_j^\dagger\hat{a}_i\hat{a}_k^\dagger\hat{a}_l\hat{a}_\alpha^\dagger\hat{a}_\beta\,|n\rangle \tag{109}$$

$$= \sum_{\alpha,\beta}\rho_{\alpha,\beta}[\delta_{m,k}\delta_{l,\alpha}\delta_{\beta,j}\delta_{i,n} - \delta_{m,j}\delta_{i,k}\delta_{l,\alpha}\delta_{\beta,n}] \tag{110}$$

similarly for the second commutator

$$\langle m|\left[S_{k,l},\hat{\rho}(t)S^{\dagger}_{i,j}\right]|n\rangle = \sum_{\alpha,\beta}\rho_{\alpha,\beta}\left\langle m\right|\left[\hat{a}^{\dagger}_{k}\hat{a}_{l},\hat{a}^{\dagger}_{\alpha}\hat{a}_{\beta}\hat{a}^{\dagger}_{j}\hat{a}_{i}\right]\left|n\right\rangle \tag{111}$$

$$= \sum_{\alpha,\beta}\rho_{\alpha,\beta}[\delta_{m,k}\delta_{l,\alpha}\delta_{\beta,j}\delta_{i,n} - \delta_{m,\alpha}\delta_{\beta,j}\delta_{i,k}\delta_{l,n}] \tag{112}$$

subbing into the full expression for Γ we find

$$\begin{aligned}\langle m|\dot{\hat{\rho}}(t)|n\rangle = \sum_{i,j,k,l,\alpha,\beta}\exp\left(-i\Delta Et\right)\Gamma_{i,j;k,l}(\omega_{k,l})\rho_{\alpha,\beta}[\quad & \delta_{m,k}\delta_{l,\alpha}\delta_{\beta,j}\delta_{i,n} \\ & -\delta_{m,j}\delta_{i,k}\delta_{l,\alpha}\delta_{\beta,n}] \\ +\exp\left(i\Delta Et\right)\Gamma^{*}_{k,l;i,j}(\omega_{i,j})\rho_{\alpha,\beta}[\quad & \delta_{m,k}\delta_{l,\alpha}\delta_{\beta,j}\delta_{i,n} \\ & -\delta_{m,\alpha}\delta_{\beta,j}\delta_{i,k}\delta_{l,n}]\end{aligned} \tag{113}$$

C.1 Rotating Wave Approximation

To apply the rotating wave approximation we consider two cases

- $i = j$, $k = l$
- $i = k$, $j = l$

however we need to make sure we don't double count. This is done using the following delta function $\delta_{i,j}\delta_{k,l} + \delta_{i,k}\delta_{j,l} - \delta_{i,j}\delta_{k,l}\delta_{i,k}$ applied to each group of δ functions separately

$$(1) = (\delta_{i,j}\delta_{k,l} + \delta_{i,k}\delta_{j,l} - \delta_{i,j}\delta_{k,l}\delta_{i,k})(\delta_{m,k}\delta_{l,\alpha}\delta_{\beta,j}\delta_{i,n}) \tag{114}$$

$$= (\delta_{m,k,l,\alpha}\delta_{\beta,j,i,n} + \delta_{i,n,m,k}\delta_{l,\alpha,\beta,j} - \delta_{m,k,l,\alpha,\beta,j,i,n}) \tag{115}$$

$$(2) = (\delta_{i,j}\delta_{k,l} + \delta_{i,k}\delta_{j,l} - \delta_{i,j}\delta_{k,l}\delta_{i,k})(\delta_{m,j}\delta_{i,k}\delta_{l,\alpha}\delta_{\beta,n}) \tag{116}$$

$$= (\delta_{m,j,i,k,l,\alpha}\delta_{\beta,n} + \delta_{m,j,l,\alpha}\delta_{i,k}\delta_{\beta,n} - \delta_{m,j,i,k,l,\alpha}\delta_{\beta,n}) \tag{117}$$

$$(3) = (\delta_{i,j}\delta_{k,l} + \delta_{i,k}\delta_{j,l} - \delta_{i,j}\delta_{k,l}\delta_{i,k})(\delta_{m,\alpha}\delta_{\beta,j}\delta_{i,k}\delta_{l,n}) \tag{118}$$

$$= (\delta_{m,\alpha}\delta_{\beta,j,i,k,l,n} + \delta_{m,\alpha}\delta_{\beta,j,l,n}\delta_{i,k} - \delta_{m,\alpha}\delta_{\beta,j,i,k,l,n}) \tag{119}$$

applying this to the full expression we find

$$\begin{aligned}\langle m|\,\dot{\hat{\rho}}(t)\,|n\rangle = \sum_{i,j,k,l,\alpha,\beta} & \Gamma_{i,j;k,l}(\omega_{k,l})\rho_{\alpha,\beta}[\\ & (\delta_{m,k,l,\alpha}\delta_{\beta,j,i,n} + \delta_{i,n,m,k}\delta_{l,\alpha,\beta,j} - \delta_{m,k,l,\alpha,\beta,j,i,n}) \\ & -(\delta_{m,j,i,k,l,\alpha}\delta_{\beta,n} + \delta_{m,j,l,\alpha}\delta_{i,k}\delta_{\beta,n} - \delta_{m,j,i,k,l,\alpha}\delta_{\beta,n})] \\ & +\Gamma^*_{k,l;i,j}(\omega_{i,j})\rho_{\alpha,\beta}[\\ & (\delta_{m,k,l,\alpha}\delta_{\beta,j,i,n} + \delta_{i,n,m,k}\delta_{l,\alpha,\beta,j} - \delta_{m,k,l,\alpha,\beta,j,i,n}) \\ & -(\delta_{m,\alpha}\delta_{\beta,j,i,k,l,n} + \delta_{m,\alpha}\delta_{\beta,j,l,n}\delta_{i,k} - \delta_{m,\alpha}\delta_{\beta,j,i,k,l,n})]\end{aligned} \tag{120}$$

$$\begin{aligned}= \sum_i [& (\Gamma_{n,n;m,m}(\omega_{m,m})\rho_{m,n}\delta_{i,n} + \Gamma_{n,i;n,i}(\omega_{n,i})\rho_{i,i}\delta_{m,n} \\ & -\Gamma_{n,n;n,n}(\omega_{n,n})\rho_{n,n}\delta_{m,n,i}) \\ & -(\Gamma_{m,m;m,m}(\omega_{m,m})\rho_{m,n}\delta_{i,n} + \Gamma_{i,m;i,m}(\omega_{i,m})\rho_{m,n} \\ & -\Gamma_{m,m;m,m}(\omega_{m,m})\rho_{m,n}\delta_{i,n})] \\ & +[(\Gamma^*_{m,m;n,n}(\omega_{n,n})\rho_{m,n}\delta_{i,n} + \Gamma^*_{m,i;m,i}(\omega_{m,i})\rho_{i,i}\delta_{n,m} \\ & -\Gamma^*_{n,n,n,n}(\omega_{n,n})\rho_{n,n}\delta_{n,m,i}) \\ & -(\Gamma^*_{n,n;n,n}(\omega_{n,n})\rho_{m,n}\delta_{i,n} + \Gamma^*_{i,n;i,n}(\omega_{i,n})\rho_{m,n} \\ & -\Gamma^*_{n,n,n,n}(\omega_{n,n})\rho_{m,n}\delta_{i,n})]\end{aligned} \tag{121}$$

$$\begin{aligned}= \sum_i [& \Gamma_{n,n;m,m}(\omega_{m,m})\rho_{m,n}\delta_{i,n} + \Gamma_{n,i;n,i}(\omega_{n,i})\rho_{i,i}\delta_{m,n} \\ & -\Gamma_{n,n;n,n}(\omega_{n,n})\rho_{n,n}\delta_{m,n,i} - \Gamma_{i,m;i,m}(\omega_{i,m})\rho_{m,n}] \\ & +[\Gamma^*_{m,m;n,n}(\omega_{n,n})\rho_{m,n}\delta_{i,n} + \Gamma^*_{m,i;m,i}(\omega_{m,i})\rho_{i,i}\delta_{n,m} \\ & -\Gamma^*_{n,n,n,n}(\omega_{n,n})\rho_{n,n}\delta_{n,m,i} - \Gamma^*_{i,n;i,n}(\omega_{i,n})\rho_{m,n}]\end{aligned} \tag{122}$$

to convert Γ^* into Γ we use $\Gamma^*_{a,b,c,d} = \Gamma_{c,d,a,b}$

$$\begin{aligned}\langle m|\,\dot{\hat{\rho}}(t)\,|n\rangle = \sum_i [& \Gamma_{n,n;m,m}(\omega_{m,m})\rho_{m,n}\delta_{i,n} + \Gamma_{n,i;n,i}(\omega_{n,i})\rho_{i,i}\delta_{m,n} \\ & -\Gamma_{n,n;n,n}(\omega_{n,n})\rho_{n,n}\delta_{m,n,i} - \Gamma_{i,m;i,m}(\omega_{i,m})\rho_{m,n}] \\ & +[\Gamma_{n,n;m,m}(\omega_{m,m})\rho_{m,n}\delta_{i,n} + \Gamma_{m,i;m,i}(\omega_{m,i})\rho_{i,i}\delta_{n,m} \\ & -\Gamma_{n,n,n,n}(\omega_{n,n})\rho_{n,n}\delta_{n,m,i} - \Gamma_{i,n;i,n}(\omega_{n,i})\rho_{m,n}]\end{aligned} \tag{123}$$

$$\begin{aligned}= \sum_i [& 2\Gamma_{n,n;m,m}(\omega_{m,m})\rho_{m,n}\delta_{i,n} + 2\Gamma_{n,i;n,i}(\omega_{n,i})\rho_{i,i}\delta_{m,n} \\ & -2\Gamma_{n,n;n,n}(\omega_{n,n})\rho_{n,n}\delta_{m,n,i} - \Gamma_{i,m;i,m}(\omega_{i,m})\rho_{m,n} \\ & -\Gamma_{i,n;i,n}(\omega_{n,i})\rho_{m,n}]\end{aligned} \tag{124}$$

the second and third terms cancel for $i = m$, and the first and last two terms cancel for $m = n$ provided $i = n$

$$\langle m|\,\dot{\hat{\rho}}(t)\,|n\rangle = \sum_i [2\Gamma_{n,n;m,m}(\omega_{m,m})\rho_{m,n}\delta_{i,n} + 2\Gamma_{n,\neq n;n,\neq n}(\omega_{n,\neq n})\rho_{\neq n,\neq n}\delta_{m,n,i} - \Gamma_{i,m;i,m}(\omega_{i,m})\rho_{m,n} - \Gamma_{i,n;i,n}(\omega_{n,i})\rho_{m,n}] \tag{125}$$

If we take $m = n$

$$\begin{aligned}\langle m|\,\dot{\hat{\rho}}(t)\,|m\rangle &= \sum_{i,n\neq m} [2\Gamma_{m,m;m,m}(\omega_{m,m})\rho_{m,m}\delta_{i,m} && (126)\\ &\qquad + 2\Gamma_{m,n;m,n}(\omega_{m,n})\rho_{n,n}\delta_{m,i} \\ &\qquad - 2\Gamma_{i,m;i,m}(\omega_{i,m})\rho_{m,m}] \\ &= 2\sum_{i,n\neq m} [\Gamma_{m,n;m,n}(\omega_{m,n})\rho_{n,n}\delta_{m,i} && (127)\\ &\qquad - \Gamma_{n,m;n,m}(\omega_{n,m})\rho_{m,m}\delta_{m,i}] \\ &= 2\sum_{n\neq m} [\Gamma_{m,n;m,n}(\omega_{m,n})\rho_{n,n} - \Gamma_{n,m;n,m}(\omega_{n,m})\rho_{m,m}] && (128)\end{aligned}$$

If we take $m \neq n$

$$\langle m|\,\dot{\hat{\rho}}(t)\,|\neq m\rangle = \sum_i [2\Gamma_{\neq m,\neq m;m,m}(\omega_{m,m})\rho_{m,\neq m}\delta_{i,m} - \Gamma_{i,m;i,m}(\omega_{i,m})\rho_{m,\neq m} - \Gamma_{i,\neq m;i,\neq m}(\omega_{i,\neq m,})\rho_{m,\neq m}] \tag{129}$$

We only have self interaction in the diagonal elements. If they start 0 they will always remain zero at later times. If we sum over m for the case $n = m$ we find the total derivative is zero, the normalisation of the density matrix is preserved.

C.2 Full Solution

The full solution to the equation is much more complicated. Starting from the previous expression for ρ we swap Γ^* for Γ and expand

$$\begin{aligned}\langle m|\,\dot{\hat{\rho}}(t)\,|n\rangle = \sum_{i,j,k,l,\alpha,\beta} &\exp\left(-i\Delta E_{i,j;k,l}t\right)\Gamma_{i,j;k,l}(\omega_{k,l})\rho_{\alpha,\beta}[\\ &\delta_{m,k}\delta_{l,\alpha}\delta_{\beta,j}\delta_{i,n} - \delta_{m,j}\delta_{i,k}\delta_{l,\alpha}\delta_{\beta,n}] \\ &+\exp\left(i\Delta E_{i,j;k,l}t\right)\Gamma_{i,j;k,l}(\omega_{i,j})\rho_{\alpha,\beta}[\\ &\delta_{m,k}\delta_{l,\alpha}\delta_{\beta,j}\delta_{i,n} - \delta_{m,\alpha}\delta_{\beta,j}\delta_{i,k}\delta_{l,n}]\end{aligned} \tag{130}$$

$$\begin{aligned}= \sum_{i,j} &\exp\left(-i\Delta E_{n,j;m,i}t\right)\Gamma_{n,j;m,i}(\omega_{m,i})\rho_{i,j} \\ &-\exp\left(-i\Delta E_{i,m;i,j}t\right)\Gamma_{i,m;i,j}(\omega_{i,j})\rho_{j,n} \\ &+\exp\left(i\Delta E_{n,j;m,i}t\right)\Gamma_{n,j;m,i}(\omega_{n,j})\rho_{i,j} \\ &-\exp\left(i\Delta E_{i,j;i,n}t\right)\Gamma_{i,j;i,n}(\omega_{i,j})\rho_{m,j}\end{aligned} \tag{131}$$

consider the case $m = n$

$$\begin{aligned}\langle m|\,\dot{\hat{\rho}}(t)\,|m\rangle = \sum_{i,j} &\exp\left(-i\omega_{i,j}t\right)\Gamma_{m,j;m,i}(\omega_{m,i})\rho_{i,j} \\ &-\exp\left(-i\omega_{j,m}t\right)\Gamma_{i,m;i,j}(\omega_{i,j})\rho_{j,m} \\ &+\exp\left(i\omega_{i,j}t\right)\Gamma_{m,j;m,i}(\omega_{m,j})\rho_{i,j} \\ &-\exp\left(i\omega_{m,j}t\right)\Gamma_{i,j;i,m}(\omega_{i,j})\rho_{m,j}\end{aligned} \tag{132}$$

$$\begin{aligned}= \sum_{i,j} &(\exp\left(-i\omega_{i,j}t\right)\Gamma_{m,j;m,i}(\omega_{m,i}) + \exp\left(i\omega_{i,j}t\right)\Gamma_{m,j;m,i}(\omega_{m,j}))\rho_{i,j} \\ &-\exp\left(-i\omega_{j,m}t\right)\Gamma_{i,m;i,j}(\omega_{i,j})(\rho_{j,m} + \rho_{m,j})\end{aligned} \tag{133}$$

we need to make sure that this has no contribution for $\Gamma(0)$, as this is divergent (see eq. (181)). We only need to worry about terms not already covered by the rotating wave approximation. This covers only one case for each part of the expression

- $i \neq j$, $i \neq m$ in the first expression
- $j \neq m$, $i \neq j$ on the second etc ...

the contribution from these terms is then

$$\begin{aligned}&\exp\left(-i\omega_{\neq m,m}t\right)\Gamma_{m,m;m,\neq m}(\omega_{m,\neq m})\rho_{\neq m,m} \\ &+\exp\left(i\omega_{m,\neq m}t\right)\Gamma_{m,\neq m;m,m}(\omega_{m,\neq m})\rho_{m,\neq m} \\ &-\exp\left(-i\omega_{\neq m,m}t\right)\Gamma_{m,m;m,\neq m}(\omega_{m,\neq m})(\rho_{\neq m,m} + \rho_{m,\neq m})\end{aligned} \tag{134}$$

It is clear that these terms all cancel, and the divergence of Γ at $\omega = 0$ has no effect on the diagonal terms of the density matrix. By a similar process the same can be shown for cross diagonal terms.

D Calculating the Lindblad Rate Constant

Starting from the definition of the Lindblad rate constant γ (eq. (43)) and the environment interaction hamiltonian (eq. (32)) we find

$$\Gamma_{i,j,k,l}(\omega) = \int_0^\infty ds \exp(i\omega s) Tr_E[E^\dagger_{i,j}(t) E_{k,l}(t-s)\rho_E(0)] \tag{135}$$

where

$$E_{i,j}(t) = \exp(iH_e t) \sum_{k,k'} V_{i,j} \hat{b}^\dagger_{k',s'} \hat{b}_{k,s} \exp(-iH_e t) \tag{136}$$

$$= \sum_{k,k'} \hat{V}_{i,j} \hat{b}^\dagger_{k',s'} \hat{b}_{k,s} \exp(i(E'_k - E_k)t) \tag{137}$$

For a purely statistical ensemble of electrons the density matrix is diagonal [22]

$$\rho_E(0) = \sum_{\{N(k)\}} P(\{N(k)\}) |N(k)\rangle \langle N(k)| \tag{138}$$

where $P(N(k)) = \frac{1}{z}\sum_{k,s} \exp(-N(k)_s(\beta E_k - \mu))$.

We start by expanding out the trace over the environment

$$Tr_E[\dots] = \sum_{\{N(k)\}} \langle N(k)| E^\dagger_{i,j}(t) E_{k,l}(t-s)\rho_E(0) |N(k)\rangle \tag{139}$$

$$= \sum_{\{N(k)\},\{N'(k)\}} P(\{N'(k)\}) \langle N'(k)| |N(k)\rangle \tag{140}$$
$$\langle N(k)| E^\dagger_{i,j}(t) E_{k,l}(t-s) |N'(k)\rangle$$

$$= \sum_{\{N(k)\}} P(\{N(k)\}) \langle N(k)| E^\dagger_{i,j}(t) E_{k,l}(t-s) |N(k)\rangle \tag{141}$$

$$= \sum_{\substack{\{N(k)\} \\ k_1,s^1,k_2,s^2 \\ k_3,s^3,k_4,s^4}} P(\{N(k)\}) V_{i,j} V_{k,l} \tag{142}$$
$$\exp(i(E_1 - E_2)t) \exp(i(E_3 - E_4)(t-s))$$
$$\langle N(k)| \hat{b}^\dagger_{k_1,s^1} \hat{b}_{k_2,s^2} \hat{b}^\dagger_{k_3,s^3} \hat{b}_{k_4,s^4} |N(k)\rangle$$

Where here we have used the fact that the potential is real, and swapped the order of k_1, k_2 from the usual definition. This expression is non zero in only two cases

- $k_1 = k_2, s^1 = s^2$, $k_3 = k_4, s^3 = s^4$
- $k_1 = k_4, s^1 = s^4$, $k_3 = k_2, s^3 = s^2$ but $k_1 \neq k_2, s^1 \neq s^2$

we use the result

$$\langle N(k)|\,\hat{b}^{\dagger}_{k_1,s^1}\hat{b}_{k_1,s^1}\hat{b}^{\dagger}_{k_3,s^3}\hat{b}_{k_3,s^3}\,|N(k)\rangle = N_1N_3 \tag{143}$$

$$\langle N(k)|\,\hat{b}^{\dagger}_{k_1,s^1}\hat{b}_{k_3,s^3}\hat{b}^{\dagger}_{k_3,s^3}\hat{b}_{k_1,s^1}\,|N(k)\rangle = \langle N(k)|\,\hat{b}^{\dagger}_{k_1,s^1}\hat{b}_{k_1,s^1}\hat{b}_{k_3,s^3}\hat{b}^{\dagger}_{k_3,s^3}\,|N(k)\rangle \tag{144}$$

$$= N_1(1-N_3) \tag{145}$$

to simplify the above sum

$$Tr_E[\dots] = \sum_{k_1,s^1,k_3,s^3} V_{i,j}V_{k,l}[\tag{146}$$
$$N_1N_3 + N_1(1-N_3)\exp\left(-i(E_3-E_1)s\right)]$$

If we then integrate over s we find

$$\Gamma_{i,j,k,l}(\omega) = \int_0^{\infty} ds\exp\left(i\omega s\right)Tr_E[\dots] \tag{147}$$

$$= \sum_{\substack{k_1,s^1,k_3,s^3\\ k_4,s^4}} V_{i,j}V_{k,l}[N_1N_3\delta(w) + N_1(1-N_3)\delta(w+E_1-E_3)] \tag{148}$$

to convert these delta functions into delta function in momentum we use the formula $\delta(f(x)) = |\frac{df}{dx}|^{-1}\delta(x-x_0)$ to give

$$\delta(w+E_1-E_3) = \frac{m_e}{\sqrt{k_1^2-2m_e\omega}}\delta(k_3 \pm \sqrt{k_1^2+2m_e\omega}) \tag{149}$$

Note we are working in units of $\hbar = 1$ and the $\delta(\omega)$ is just constraining $E_3 = E_4$ which is already satisfied when $k_3 = k_4$. Adding this back into the expression for Γ we find

$$\Gamma_{i,j,k,l}(\omega) = \sum_{k_1,s^1,k_3,s^3} V_{i,j}V_{k,l}[N_1N_3\delta_{w,0}\frac{m_e}{\sqrt{k_3^2}} \tag{150}$$
$$+ N_1(1-N_3)\frac{m_e}{\sqrt{k_1^2-2m_e\omega}}\delta(k_3 \pm \sqrt{k_1^2+2m_e\omega})]$$

To calculate these terms we need to switch to the integral representation. Absorbing the factors of L^6 back into the definition of $V_{i,j}$ we find

$$\Gamma_{i,j,k,l}(\omega) = \sum_{s^1,s^3}\int \frac{d^3\mathbf{k}_1}{(2\pi)^3}\frac{d^3\mathbf{k}_3}{(2\pi)^3}V_{i,j}V_{k,l}[N_1N_3\delta_{w,0}\frac{m_e}{\sqrt{k_3^2}} \tag{151}$$
$$+ N_1(1-N_3)\frac{m_e}{\sqrt{k_1^2-2m_e\omega}}\delta(k_3 \pm \sqrt{k_1^2+2m_e\omega})]$$

we perform the integral over k by expanding about $k = k_f$ noting that the value of ω is equal to the energy difference of the hydrogen $\Gamma_{i,j,k,l}(\omega) = \Gamma_{i,j,k,l}(\omega_{k,l})$

where $\omega_{k,l} = E_k - E_l$ (see eq. (128)).

$$1 - N_3 = \frac{1}{1 + \exp(-\beta(E_3 - \mu))} \tag{152}$$

$$= \frac{1}{1 + \exp(-\beta(E_1 + \omega - \mu))} \tag{153}$$

$$\sim \frac{1}{2 + -\beta(E_1 + \omega - \mu)} \tag{154}$$

$$\sim \frac{1}{(1 - \frac{\beta\omega}{2})(2 + -\beta(E_1 - \mu))} \tag{155}$$

$$\sim \exp(\frac{\beta\omega}{2}) \frac{1}{1 + \exp(-\beta(E_1 - \mu))} \tag{156}$$

We then discard the first part of the integral by noting no terms with $\omega = 0$ appear in the final expression for $\dot{\rho}$, and note $\omega \ll k_1$ at the fermi surface.

$$\Gamma_{i,j,k,l}(\omega_{k,l}) = \sum_{s^1,s^3} \exp(\frac{\beta\omega_{k,l}}{2}) \int \frac{m_e (4\pi)^2 k_1^4 dk_1}{(2\pi)^6 \sqrt{k_1^2 - 2m_e\omega}} V_{i,j} V_{k,l} [N_1(1 - N_1)] \tag{157}$$

$$= \sum_{s^1,s^3} \exp(\frac{\beta\omega_{k,l}}{2}) \int \frac{m_e k_1^3 dk_1}{4\pi^4} V_{i,j} V_{k,l} [N_1(1 - N_1)] \tag{158}$$

we expand $N_1(1 - N_1)$ about $k_1 = k_f$

$$N_1(1 - N_1) = \frac{1}{1 + \exp \beta\Delta E} \frac{1}{1 + \exp -\beta\Delta E} \tag{159}$$

$$\sim \frac{1}{2 + \beta\Delta E + \frac{(\beta\Delta E)^2}{2}} \frac{1}{2 - \beta\Delta E + \frac{(\beta\Delta E)^2}{2}} \tag{160}$$

$$= \frac{1}{4} \frac{1}{1 + \frac{\beta\Delta E}{2} + \frac{(\beta\Delta E)^2}{4}} \frac{1}{1 - \frac{\beta\Delta E}{2} + \frac{(\beta\Delta E)^2}{4}} \tag{161}$$

$$\sim \frac{1}{4}(1 - \frac{\beta\Delta E}{2} - \frac{(\beta\Delta E)^2}{4} + (\frac{\beta\Delta E}{2})^2) \tag{162}$$

$$(1 + \frac{\beta\Delta E}{2} - \frac{(\beta\Delta E)^2}{4} + (\frac{\beta\Delta E}{2})^2)$$

$$= \frac{1}{4}(1 - \frac{(\beta\Delta E)^2}{4}) \tag{163}$$

$$\sim \frac{1}{4} \exp(-\frac{(\beta\Delta E)^2}{4}) \tag{164}$$

The sharp exponential decay justifies this expansion. Going back to the integral

we have

$$\Gamma_{i,j,k,l}(\omega_{k,l}) = \sum_{s^1,s^3} \exp\left(\frac{\beta\omega_{k,l}}{2}\right) \int \frac{m_e k_1^3 dk_1}{(2\pi)^4} V_{i,j} V_{k,l} \exp\left(-\frac{(\beta\Delta E)^2}{4}\right) \tag{165}$$

$$= \sum_{s^1,s^3} \exp\left(\frac{\beta\omega_{k,l}}{2}\right) \int \frac{m_e k_1^3 dk_1}{(2\pi)^4} V_{i,j} V_{k,l} \exp\left(-\frac{\left(\frac{\beta\hbar^2}{2m_e}(k_1^2 - k_f^2)\right)^2}{4}\right) \tag{166}$$

$$= \sum_{s^1,s^3} \exp\left(\frac{\beta\omega_{k,l}}{2}\right) \int \frac{m_e k_f^2 du}{2(2\pi)^4} V_{i,j} V_{k,l} \exp\left(-\frac{\beta^2\hbar^4}{(4m_e)^2} u^2\right) \tag{167}$$

$$= \sum_{s^1,s^3} \exp\left(\frac{\beta\omega_{k,l}}{2}\right) \frac{m_e k_f^2}{(2\pi)^4} V_{i,j} V_{k,l} \sqrt{\pi} \frac{2m_e}{\beta\hbar^2} \tag{168}$$

checking the units of Γ we find

$$[\Gamma] = [kg]^2 [m^{-2}] [kgm^5 s^{-2}]^2 [kgm^2 s^{-2}]^1 [kgm^2 s^{-1}]^{-2} \tag{169}$$

$$= [kg^2 m^{-2} m^6 s^{-2} kg^1 m^2 s^{-2}] \tag{170}$$

$$= [kg^3 m^6 s^{-4}] \tag{171}$$

to recover the correct units of s^{-1} we therefore divide by $\hbar^3$ which was previously taken to be 1. We can also write $V_{i,j} = \mathcal{C}_{i,j} \frac{2e^2}{\epsilon_0 \alpha^2} = \mathcal{C}_{i,j} \frac{8\pi^2 \epsilon_0 \hbar^4}{e^2 m_e^2}$ where $\mathcal{C}_{i,j}$ is the hydrogen overlap factor given in section 2.6

$$\Gamma_{i,j,k,l}(\omega_{k,l}) = \sum_{s^1,s^3} \exp\left(\frac{\beta\omega_{k,l}}{2}\right) \frac{m k_f^2}{(2\pi)^4} \mathcal{C}_{i,j} \mathcal{C}_{k,l} \sqrt{\pi} \frac{2m}{\beta\hbar^5} \left(\frac{8\pi^2 \epsilon_0 \hbar^4}{e^2 m_e^2}\right)^2 \tag{172}$$

$$= \sum_{s^1,s^3} \exp\left(\frac{\beta\omega_{k,l}}{2}\right) \mathcal{C}_{i,j} \mathcal{C}_{k,l} \sqrt{\pi} \frac{8 k_f^2 \epsilon_0^2 \hbar^3}{\beta e^4 m_e^2} \tag{173}$$

D.1 $\omega = 0$ contribution

If we go back to calculate the $\omega = 0$ contribution we find (by taking the low temperature limit and noting particle number is constant with temperature)

$$\Gamma_{i,j,k,l}(\omega) = \sum_{s^1,s^3} \int_0^{k_f} \frac{d^3\mathbf{k}_1}{(2\pi)^3} \frac{d^3\mathbf{k}_3}{(2\pi)^3} V_{i,j} V_{k,l} [N_1 N_3 \delta_{w,0} \frac{m_e}{k_3}] \tag{174}$$

$$= \sum_{s^1,s^3} \int_0^{k_f} \frac{4\pi k_1^2 dk_1}{(2\pi)^3} \frac{4\pi m_e k_3 dk_3}{(2\pi)^3} V_{i,j} V_{k,l} \delta_{w,0} \tag{175}$$

$$= \sum_{s^1,s^3} \frac{4\pi k_f^3 m_e}{3(2\pi)^3} \frac{2\pi k_f^2}{(2\pi)^3} V_{i,j} V_{k,l} \delta_{w,0} \tag{176}$$

$$= \sum_{s^1,s^3} \frac{4\pi k_f^3 m_e}{3(2\pi)^3} \frac{2\pi k_f^2}{(2\pi)^3} V_{i,j} V_{k,l} \delta_{w,0} \tag{177}$$

$$\tag{178}$$

If we add back in the factor of $\hbar^3$

$$\Gamma_{i,j,k,l}(0) = \sum_{s^1,s^3} \frac{4\pi k_f^3 m_e}{3\hbar^3(2\pi)^3} \frac{2\pi k_f^2}{(2\pi)^3} \mathcal{C}_{i,j} \mathcal{C}_{k,l} \delta_{w,0} (\frac{8\pi^2 \epsilon_0 \hbar^4}{e^2 m_e^2})^2 \tag{179}$$

$$= \sum_{s^1,s^3} \frac{8 k_f^5 \epsilon_0^2 \hbar^5}{3 e^4 m_e^3} \mathcal{C}_{i,j} \mathcal{C}_{k,l} \delta_{w,0} \tag{180}$$

If we use dimensional analysis on this term we find it is proportional to $m^{-1}s^{-1}$. This is because we have ignored an important subtlety when imposing the ω delta function. If we had done it properly (before setting $k_3 = k_4$) we would get out an extra factor of L. This term therefore diverges as $L \to \infty$.

$$\Gamma_{i,j,k,l}(\omega) = L \sum_{s^1,s^3} \frac{8 k_f^5 \epsilon_0^2 \hbar^5}{3 e^4 m_e^3} \mathcal{C}_{i,j} \mathcal{C}_{k,l} \delta_{w,0} \tag{181}$$